IEEE Access
Multidisciplinary ⋮ Rapid Review ⋮ Open Access Journal

Received January 17, 2020, accepted February 19, 2020, date of publication March 4, 2020, date of current version March 17, 2020.

*Digital Object Identifier 10.1109/ACCESS.2020.2977558*

# Stochastic Data Association for Multipath Assisted Positioning Using a Single Transmitter

**ROSTISLAV KARÁSEK[1,2] AND CHRISTIAN GENTNER[1]**

[1]German Aerospace Center (DLR), Institute of Communications and Navigation, 82334 Wessling, Germany
[2] Faculty of Electrical Engineering, Department of Electromagnetic Field, Czech Technical University in Prague, 16627 Prague, Czech Republic

Corresponding author: Rostislav Karásek (rostislav.karasek@dlr.de)

This work was supported in part by the CTU Grant SGS19/168/OHK3/3T/13 *Electromagnetic structures and waves* and in part by the DLR project *Navigation 4.0*.

**ABSTRACT** This paper builds on and extends the Channel-SLAM algorithm which exploits a multipath radio channel for the position estimation of mobile receivers. Channel-SLAM treats Multipath Components (MPCs) as Line-of-sight (LoS) signals originating from Virtual Transmitters (VTs) and estimates the positions of VTs and receiver simultaneously based on Bayesian filtering. The current Channel-SLAM implementation does not involve the retracking of previous MPCs or VTs. Therefore, when the tracking of an MPC is lost and, subsequently, regained, the corresponding VT is initialized without any prior information. Incorporating a stochastic data association algorithm extends Channel-SLAM and enables the retracking of VTs even when the MPC has been lost. The proposed algorithm increases positioning reliability, decreases computation complexity, and improves the precision of Channel-SLAM. Additionally, this paper presents a novel transition model using inertial sensors for a hand-held device for moving pedestrians. The developed positioning algorithm is evaluated based on measurement data obtained in an indoor scenario using an off-the-shelf Ultra-WideBand (UWB) module. Evaluations show that accurate position estimation can be done using only one physical transmitter and without requiring any knowledge of the physical transmitter position.

**INDEX TERMS** Channel-SLAM, data association, navigation, multipath assisted positioning, multipath channels, particle filters, pedestrian navigation, ultra wideband technology.

## I. INTRODUCTION

Knowing the precise position of an object has always been a huge advantage in many human endeavors. With the successful launch of the Sputnik 1 satellite, the Soviet Union initiated a new era of navigation. Shortly thereafter, William H. Guier and George C. Weiffenbach used the Doppler shift of Sputnik's signal to obtain the position of the receiver. Their groundbreaking work gave birth to the Global Positioning System (GPS) which was the first Global Navigation Satellite System (GNSS) [1]. Today, most smartphones are equipped with GNSS receivers which allow applications on smartphones to be used for navigation and provide sufficient position accuracy for mass-market applications in open sky conditions. However, in indoor environments, received GNSS signals may be blocked, degraded by Non-line-of-sight (NLoS) propagation or received with low power. Hence, rather than relying on GNSSs in indoor environments, different methods and sensor systems are used to obtain a position estimate. Currently, Wireless Local Area Network (WLAN), Bluetooth Low Energy (BLE), and UWB are commonly used for indoor navigation. Using WLAN for indoor positioning is a common approach because WLAN infrastructure is widely deployed. Most WLAN position estimation algorithms use Received Signal Strength Indication (RSSI) from different WLAN transmitters. Positioning systems relying on BLE for indoor positioning use RSSI and the new techniques of Angle of Arrival (AoA) and Angle of Departure (AoD) [2]. UWB positioning systems use a high bandwidth to obtain distance estimates at the cm level to allow positioning accuracy in the cm domain to be obtained in indoor environments.

The associate editor coordinating the review of this manuscript and approving it for publication was Matti Hämäläinen.


This work is licensed under a Creative Commons Attribution 4.0 License. For more information, see https://creativecommons.org/licenses/by/4.0/

All the systems mentioned above also suffer from signal blockage and degradation by NLoS propagation. A common problem in an indoor scenario is multipath propagation of the radio signal. This effect is caused by reflection and the scattering of the transmitted radio signal. Hence, the received signal does not consist only of the direct, LoS, signal, but also of multiple delayed NLoS replicas with different complex amplitudes and delays. The radio channel model linked with this form of signal distortion is called a multipath radio channel and each of the signal replicas in the received transmission is called an MPC.

A delay estimation problem arises when MPCs degrade the ability of the system to determine the delay of the LoS path. If the differences in propagation time between MPCs are less than the reciprocal of the transmission bandwidth, the MPCs are observed as the envelope of their sum. Standard distance estimation methods cannot resolve multipath propagation and are biased in multipath propagation environments.

The positioning error caused by multipath propagation effects have led to the development of a method called fingerprinting which is based on a database of signal measurements and corresponding positions. Thus, when a receiver is moving in an area with a premeasured database, the receiver compares its signal observation with the database and provides an estimated position according to the closest fit. One of the earliest works dedicated to this technique was based on an RSSI and Signal-to-Noise Ratio (SNR) measurement in a WLAN radio network with multiple transmitters [3]. The authors of [4], [5] used multipath fingerprinting for positioning.

Fingerprinting-based positioning methods require an extensive measurement campaign to obtain a database of a transmitter position or fingerprint data for its functionality. Also, each change in the environment, e.g., change of transmitter position, or rearrangement of the interior, requires the database to be updated.

However, some multipath assisted positioning algorithms do not require a fingerprinting database, e.g., the authors of [6] show that a non-static UWB radar can be used to estimate the surroundings. The extension in [7] shows that the extracted features from the environment can be further utilized for positioning using Simultaneous Localization And Mapping (SLAM). Multipath assisted positioning algorithms presented in [8]–[13], where the authors exploited MPCs for positioning using transmitter mirroring, together with a known room geometry and transmitter position using a similar principle. Transmitter mirroring is explained using the concept of the VT described in Section II-B.

Nevertheless, two techniques that do not require fingerprinting data, room geometry, nor transmitter position are at work in a multipath radio channel. The common idea of both algorithms is to assume MPCs as an LoS signal originating from so-called VTs, including the LoS signal. The only required prior information, according to SLAM theory, is the initial position of the receiver because our receiver and VT position uncertainty cannot be estimated better than the initial uncertainty of the receiver position [14]. The concept of VTs will be further explained in Section II.

The first algorithm working in a multipath radio channel is a belief propagation based on an algorithm extending the JPDA-MINT algorithm [11] which estimates user position and performing Joint Probabilistic Data Association (JPDA) of MPCs with VTs concurrently. The algorithm presented in [15] uses a SLAM technique to allow the algorithm to estimate receiver position with no knowledge of the floor plan. The JPDA-MINT (JPDA-MINT) assumes LoS and reflected signals on a wall-like obstacle while ignoring the existence of MPCs caused by the scattering of the transmitted signal. This system is modeled as a factor graph using the sum-product algorithm described in [16].

Our work is based on the Channel-SLAMchslam introduced in [17]–[20]. As with JPDA-MINT, it also uses MPCs as independent LoS signals propagating from VTs towards the receiver. On top of the JPDA-MINT algorithm, the VT model used in Channel-SLAM also includes scattering of the transmitted radio signal. In contrast to the JPDA-MINT algorithm, the estimation of position in Channel-SLAM is based on a Bayesian filtering technique. There are only two conditions that need to be fulfilled for the Channel-SLAM algorithm to converge, the existence of the static multipath radio channel environment and a moving receiver.

In this article, we propose a novel Channel-SLAM implementation for the indoor positioning of pedestrians carrying a hand-held device equipped with an Inertial Measurement Unit (IMU) and a UWB tag. It will be shown that this new approach can estimate a position accurately with only one UWB anchor by using MPCs for positioning. Compared to work before [20], we propose a Multiple Hypothesis Tracking (MHT) [21] -based data association algorithm capable of associating reappearing MPCs with corresponding VTs after an outage. The data association algorithm will be shown to improve overall precision.

The second significant change introduced in this article is a new movement model for Channel-SLAM. It expands the idea of using IMU data to improve the capability of the algorithm introduced to Channel-SLAM in [20]. A self-learning pedestrian movement model, based on a gyroscope and accelerometer measurements, will be presented. As we assume for hand-held devices, movement models for pedestrian navigation are to be utilized where the distance walked is estimated by counting steps, e.g., [22]–[24]. The proposed model is based on this technique and exploits the inference in Bayesian networks to adapt its parameters according to all available measurements. This sensor fusion helps to overcome the volatility of the model caused by random changes of step length and walking pace.

The article is structured as follows. Section II defines the signal and measurement model and describes the basic concept of the Channel-SLAM algorithm based on VTs. Section III contains the derivation of the Channel-SLAM algorithm, including data association, the incorporation of the inertial sensors' measurements into the state evolution model,

and the description of the positioning algorithm implementation. Section IV provides an experimental evaluation of the proposed algorithm precision based on simulation and measurement. We compare the proposed algorithm with the state-of-the-art Channel-SLAM algorithm [20]. The article concludes in Section V.

Throughout the paper, we use the following notations:

- $(\cdot)^{\mathrm{T}}$ stands for matrix (or vector) transpose.
- Matrices are denoted by bold letters.
- $\mathrm{A}_{lm}$ and $A_{lmo}$ represent the submatrix and element of 3-D matrix $\mathbf{A}$, respectively.
- Vector is a special case of 1-D matrix.
- $x_l$ denotes the $l$-th element of vector $\mathbf{x}$.
- $|\mathbf{x}|$ denotes the cardinality of vector $\mathbf{x}$.
- $\delta(\cdot)$ represents Dirac distribution.
- $a \sim N\left(\mu_a, \sigma_a^2\right)$ denotes the Gaussian distributed random variable $a$ with mean $\mu_a$ and variance $\sigma_a^2$.
- $\mathrm{p}\,(a)$ denotes a Probability Density Function (PDF) or Probability Mass Function (PMF) of random variable $a$
- $1:k$ stands for all integer numbers starting from 1 to $k$, thus $1, 2, \ldots, k$.
- $x_{1:k}$ is a concatenation of elements into vector $[x_1, x_2, \ldots, x_k]^{\mathrm{T}}$
- $c_0$ is the speed of light in a vacuum.
- $\hat{x}$ denotes the estimation of $x$.
- $\propto$ stands for proportional.
- $\{x^{(ij)}\}_{ij=1}^{IJ}$ defines the set consisting of two subsets for $x_{ij}$ with $i = 1, \ldots, I$, and $j = 1, \ldots, J$.
- $x^{(1:K)}$ defines the subset $\{x^{(k)}\}_{k=1}^{K}$.

## II. CONCEPT OF CHANNEL-SLAM

### A. MULTIPATH PROPAGATION

The behavior of the multipath radio channel can be described mathematically by the causal time-variant Channel Impulse Response (CIR). According to [25], the CIR can be assumed to be time-invariant for a short time interval $\delta_t = T_{t+1} - T_t$ and can be defined as a discrete function in time as

$$h_t(\tau) = \sum_{\ell=1}^{N_t} \alpha_{\ell t} \cdot \delta(\tau - \tau_{\ell t}), \tag{1}$$

where $N_t$ is the number of MPCs, $\tau_{\ell t}$ and $\alpha_{\ell t}$ are the delay and complex amplitude of the $\ell$-th MPC at time $t$. Finally, $\delta(\cdot)$ stands for the Dirac distribution [26]. By assuming that the transmitted signal $s(\tau)$ is band-limited with bandwidth $B$ and time-limited with a length smaller than $T$, the signal received at time $t$ sampled with rate $B$, bin indices $m = 0, \ldots, M-1$ and the delay $\tau_m = \frac{m}{B}$ can be expressed as

$$r_{\tau_m t} = \sum_{\ell=1}^{N_t} \alpha_{\ell t} s(\tau_m - \tau_{\ell t}) + n_{\tau_m}, \tag{2}$$

where $n_{\tau_m}$ denotes white, circular symmetric normal distributed receiver noise with variance $\sigma_n^2$. Using vector notation we obtain

$$\mathbf{r}_t = \left[r_{\tau_0 t}, \ldots, r_{\tau_m t}, \ldots, r_{\tau_{M-1} t}\right] \tag{3}$$

from (2). The CIR of (3) is represented as the sum of the delayed and weighted Dirac distributions, each representing an individual MPC with a sparse structure. However, the sparse structure of the received measured signal $\mathbf{r}_t$ is degraded by additive noise and the band-limitation of the physical transmitter and receiver hardware. To obtain the sparse structure of the CIR from $\mathbf{r}_t$, super-resolution multipath radio channel estimation algorithms are necessary.

The dynamic measurement scenario considered in this paper, with a moving receiver and a static physical transmitter, allows propagation paths to be observed for a certain time duration. This time duration depends on the physical transmitter, receiver positions, and the surrounding environment. Thus, we use a dynamic multipath radio channel estimator named Kalman Enhanced Super Resolution Tracking (KEST) [27] for estimating and tracking multipath radio channel parameters. KEST allows the evolution of CIR to be estimated over time, which is essential for Channel-SLAM, see Section II-B. KEST consists of Kalman Filters (KFs) estimating the complex amplitude $\alpha_{\ell t}$ and delay $\tau_{\ell t}$ of each MPC with respect to Maximum Likelihood (ML). The number of MPCs needs to be determined for the successful estimation and tracking of the radio channel parameters. This is known as a model order determination [27] and it is part of the KEST algorithm. KEST is using a penalized quality function, which describes the ratio between the residuals and the received signal, to decide if the model order should remain the same, should be increased, or decreased. The initial number of MPCs is obtained using the successive interference cancellation scheme similar to [28]. For further details about KEST see [27].

### B. CONCEPT OF VIRTUAL TRANSMITTERS

To use the tracked delays for positioning, a model describing the delays $\tau_{\ell t}$ dependent on current user position $\mathbf{x}_{\mathrm{Rx},t}$ is derived in [19]. We consider a static environment with a fixed physical transmitter and a receiver moving along an arbitrary trajectory. Fig. 1 shows an example of a measurement scenario where a receiver moves along the red dotted line and receives three replicas of the transmitted signal at each time step:

- The direct path shown by the solid purple lines.
- The path caused by the reflection on a wall-like obstacle indicated by the blue dashed line.
- The path linked to the scattering of the transmitted signal on an obstacle marked by the green dashed line.

Hence, the parameters of three MPCs are expected at the output of the KEST algorithm. In the case of the reflected path, the transmitted signal is reflected on a reflecting surface indicated by the solid black line. When the receiver moves, the reflection point on the reflecting surface moves as well, but if we mirror the physical transmitter position along the reflecting surface, we obtain position $\mathbf{x}_{\mathrm{Tx},2\,t}$ of $\mathrm{VT}_2$ which is static during the receiver movement. The distance between $\mathrm{VT}_2$ and the receiver is equivalent to the propagation time of the reflected signal multiplied by the speed of light. Hence,

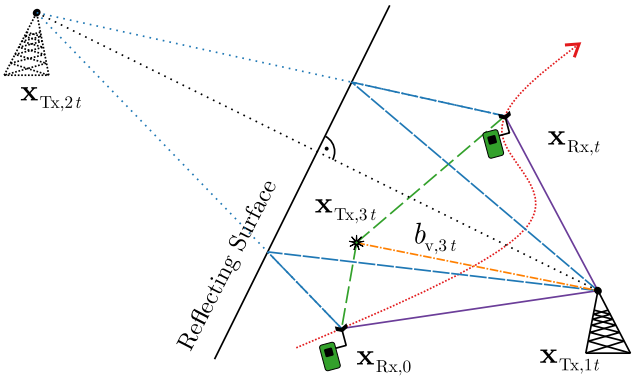


**FIGURE 1.** The concept of the Virtual Transmitters. The LoS between the physical transmitter $\mathbf{x}_{\mathrm{Tx},1\,t}$ and user trajectory in two time instances $\mathbf{x}_{\mathrm{Rx},0}$ and $\mathbf{x}_{\mathrm{Rx},t}$ is shown by solid purple lines. The MPCs caused by a reflection on a wall-like obstacle can be interpreted as an LoS signal propagated from $\mathrm{VT}_2$ at position $\mathbf{x}_{\mathrm{Tx},2\,t}$. The position of $\mathbf{x}_{\mathrm{Tx},2\,t}$ is obtained by mirroring the physical transmitter position along the reflecting surface. The real ray-like propagation is shown by the blue dashed line, while the LoS interpretation is shown by the blue dotted line. Additionally, the transmitted signal is scattered and $\mathrm{VT}_3$ is defined at the position of the scatterer $\mathbf{x}_{\mathrm{Tx},3\,t}$ and the delay of the corresponding MPC is defined as an LoS shown by the green dashed lines, with an additional propagation length $b_{\mathrm{v},3\,t}$ shown by the orange dash-dotted line.

the reflected signal can be interpreted as a direct signal propagated from $\mathrm{VT}_2$ to the receiver $\mathbf{x}_{\mathrm{Rx},t}$ shown by the blue dotted lines.

Additionally, Channel-SLAM exploits the scenario where the signal is scattered, as shown by the orange dash-dotted and green dashed lines. The propagation effect of scattering occurs if an electromagnetic wave impinges on an object (scatterer), and the energy is spread out in all directions [29]. Geometrically, the effect of scattering can be described as a fixed point at the scatterer's position in the pathway of the transmitted signal. We define $\mathrm{VT}_3$ at the position of scatterer $\mathbf{x}_{\mathrm{Tx},3\,t}$ which is constant for all receiver positions during the movement. Further, we treat $b_{\mathrm{v},3\,t} \geq 0$, the constant distance between the physical transmitter and scatterer indicated by the dash-dotted orange line, as a constant propagation length offset associated with $\mathrm{VT}_3$. Hence, the scattered signal can be interpreted as a direct signal from $\mathrm{VT}_3$ to the receiver, however, with the constant propagation length offset $b_{\mathrm{v},3\,t}$.

The concept of VT can be extended to a multiple reflection scenario and combinations of reflections and scatterings, see [19], [20]. For each of the described propagation mechanisms the $\ell$-th MPC delay can be equivalently described as a direct path between the $\mathrm{VT}_\ell$'s constant position $\mathbf{x}_{\mathrm{Tx},\ell\,t}$ and the receiver's position $\mathbf{x}_{\mathrm{Rx},t}$ plus an additional constant propagation length $b_{\mathrm{v},\ell\,t}$ . Hence,

$$d_{\ell t} = \tau_{\ell t} \cdot c_0 = \|\mathbf{x}_{\mathrm{Rx},t} - \mathbf{x}_{\mathrm{Tx},\ell\,t}\| + b_{\mathrm{v},\ell\,t}\,, \tag{4}$$

where $\mathbf{x}_{\mathrm{Tx},\ell\,t}$ is the position of the $\ell$-th VT. The position of the VTs and the additional propagation lengths are constant over time, however, for notational convenience, a time dependence on $t$ is introduced here. The additional propagation length is zero, i.e., $b_{\mathrm{v},\ell\,t} = 0$, only if reflections occur on the pathway between the physical transmitter and receiver or greater than zero, i.e., $b_{\mathrm{v},\ell\,t} > 0$, if the MPC interacts with at least one scatterer. In general, $b_{\mathrm{v},\ell\,t}/c_0$ can be interpreted as a clock offset between the $\ell$-th VT and the physical transmitter [19], [20]. The model of the VTs also holds for the physical transmitter. Hence the physical transmitter is also interpreted as a VT with unknown location.

Thus, all VTs are static while the receiver is moving, which fulfills both conditions required by the Channel-SLAM algorithm.

## III. ALGORITHM DERIVATION

In this section, we outline the essential steps of the proposed algorithm derivation whose goal is to estimate the position of user $\mathbf{x}_{\mathrm{Rx},0:t}$. To do so, we first define the state of the user as a concatenation of the user's position and other state parameters $\boldsymbol{\theta}$ which will be defined in Section III-B. So, the user state vector is

$$\mathbf{x}_{\mathrm{u},0:t} = \left[\mathbf{x}_{\mathrm{Rx},0:t}^{\mathrm{T}}, \boldsymbol{\theta}_{0:t}^{\mathrm{T}}\right]^{\mathrm{T}}. \tag{5}$$

To benefit from a multipath radio channel, the VT positions and the constant propagation length offsets have to be estimated simultaneously. Thus, we concatenate the position of $L$ VTs with the corresponding constant propagation length offsets to obtain the VTs' system state

$$\mathbf{x}_{\mathrm{v},1:L\,0:t} = \left[\mathbf{x}_{\mathrm{Tx},1:L\,0:t}^{\mathrm{T}}, b_{\mathrm{v},1:L\,0:t}\right]^{\mathrm{T}}. \tag{6}$$

The whole system is the concatenation of a receiver state with all of the VTs states denoted as

$$\mathbf{x}_{0:t} = \left[\mathbf{x}_{\mathrm{u},0:t}^{\mathrm{T}}, \mathbf{x}_{\mathrm{v},1:L\,0:t}^{\mathrm{T}}\right]^{\mathrm{T}}. \tag{7}$$

Assuming that the current state is dependent on the previous states, in time step $t$ we need to estimate the PDF of state $\mathbf{x}_t$ given all previous $\mathbf{x}_{0:t-1}$ states and all collected evidence, also known as a posterior PDF. In our work we assume two sources of evidence: the parameters of the MPCs estimated by KEST from $\mathbf{r}_{1:t}$ concatenated in measurement vector

$$\mathbf{z}_{1:t} = [\tau_{0\,1:t}, \ldots, \tau_{m\,1:t}, \ldots, \tau_{M-1\,1:t}]^{\mathrm{T}}; \tag{8}$$

and the output of the inertial sensors after calibration and processing which is then used as a control signal $\mathbf{u}_{1:t}$ as described in Section III-B. Furthermore, association variable $\mathbf{n}_{1:t}$ is used, which matches the individual MPCs with the corresponding VTs in the system state. Otherwise stated, the association variable $n_{i\,t}$ is an integer linking measurement $z_{i\,t}$ with $\mathbf{x}_{\mathrm{v},n_{i\,t}\,t}$. Assume, for example, that the measurement vector consists of three delays $\mathbf{z}_t = [1.4, 2.5, 4.4]^{\mathrm{T}}$, and the Channel-SLAM currently consists of five VTs. If the first delay is associated with the second VT in $\mathbf{x}_{\mathrm{v},\,t}$, the second delay with the fifth VT, and the third delay with the first VT, the association variable would be $\mathbf{n}_t = [2, 5, 1]^{\mathrm{T}}$.

The problem of estimating the PDF of state $\mathbf{x}_{0:t}$ at the same time as the data association results in calculating a Joint Probability Density Function (JPDF) conditioned on the collected evidence

$$\mathrm{p}\left(\mathbf{x}_{0:t}, \mathbf{n}_{1:t} \mid \mathbf{z}_{1:t}, \mathbf{u}_{1:t}\right), \tag{9}$$

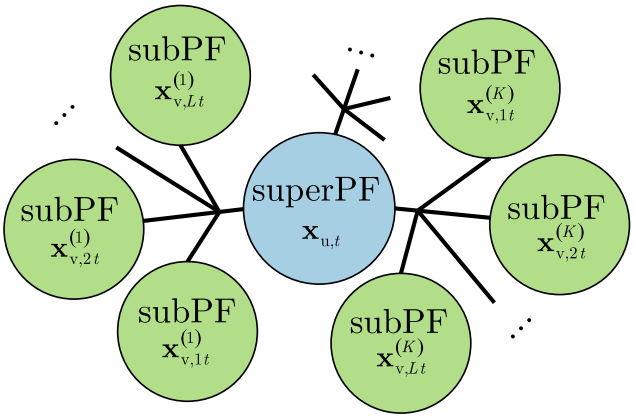


**FIGURE 2.** Graphical representation of the Rao-Blackwellized Particle Filter, where user state $\mathbf{x}_{\mathrm{u},t}$ is represented by superordinate PF, while for each user state particle $\mathbf{x}_{\mathrm{u},t}^{(k)}$ there is a set of independent subordinate PFs representing the state of the individual VTs. The state of the $p$-th particle of the $\ell$-th VT linked with $k$-th user particle is given by $\mathbf{x}_{\mathrm{v},\ell t}^{(kp)}$.

sometimes referred to as a posterior, or belief function $\mathrm{bel}\left(\mathbf{x}_{0:t}, \mathbf{n}_{1:t}\right)$.

The derivation of the proposed positioning algorithm is based on previous work [19]. The difference is that we are using the IMU-based control signals $\mathbf{u}_{1:t}$ and data association $\mathbf{n}_{1:t}$ directly during the whole derivation which will be exploited for our data association algorithm and movement model. This approach results in a slightly different derivation, but the main ideas of Channel-SLAM are preserved.

The first step during the derivation is to factorize the state posterior defined in (9) as

$$\begin{aligned}&\overbrace{\mathrm{p}\left(\mathbf{n}_{1:t} \mid \mathbf{x}_{0:t}, \mathbf{z}_{1:t}, \mathbf{u}_{1:t}\right)}^{\text{data association posterior}} \overbrace{\mathrm{p}\left(\mathbf{x}_{0:t} \mid \mathbf{z}_{1:t}, \mathbf{u}_{1:t}\right)}^{\text{state posterior}} \\ &= \overbrace{\mathrm{p}\left(\mathbf{n}_{1:t} \mid \mathbf{x}_{0:t}, \mathbf{z}_{1:t}, \mathbf{u}_{1:t}\right)}^{\text{data association posterior}} \overbrace{\mathrm{p}\left(\mathbf{x}_{\mathrm{u},0:t} \,\middle|\, \mathbf{z}_{1:t}, \mathbf{u}_{1:t}\right)}^{\text{user state posterior}} \\ &\quad \times \prod_{\ell} \underbrace{\mathrm{p}\left(\mathbf{x}_{\mathrm{v},\ell\,0:t} \,\middle|\, \mathbf{x}_{\mathrm{u},0:t}, \mathbf{z}_{1:t}, \mathbf{u}_{1:t}\right)}_{\ell\text{-th VT state posterior}}. \end{aligned} \tag{10}$$

In the beginning, the posterior is separated into the data association posterior and the state posterior using the product rule. The later posterior is further modified using the same rule to separate the state posterior into the user's $\mathbf{x}_{\mathrm{u},0:t}$ and VTs' $\mathbf{x}_{\mathrm{v},1:L\,0:t}$ posteriors. The last product term in (10) is obtained using the independence between the individual MPCs in the wireless channel. We can exploit this conditional independence to represent the user's state by a superordinate Particle Filter (PF) and each of the virtual transmitters by the set of subordinate PFs. This concept is shown in Fig. 2 where each of the $K$ particles representing $\mathbf{x}_{\mathrm{u},t}$ is assigned with the set of subordinate PFs representing $L$ VTs. This separation into the set of conditionally independent posteriors is also known as a Rao-Blackwellized Particle Filter (RBPF). For further information about the RBPF in Channel-SLAM see [19].

Now, if we look closely at the first two terms on the r.h.s. of (10), we notice that it is actually a product of a data association and user state beliefs. If we use Bayes' rule and the product rule, we obtain the term above as

$$\begin{aligned}\mathrm{bel}\left(\mathbf{n}_{1:t}\right)\mathrm{bel}\left(\mathbf{x}_{\mathrm{u},0:t}\right) = \eta\mathrm{p}\left(\mathbf{z}_t \mid \mathbf{n}_t, \mathbf{x}_t\right)\mathrm{p}\left(\mathbf{n}_t \mid \mathbf{n}_{t-1}\right) \\ \mathrm{p}\left(\mathbf{z}_t \,\middle|\, \mathbf{x}_{\mathrm{u},t}, \mathbf{z}_{t-1}\right)\mathrm{p}\left(\mathbf{x}_{\mathrm{u},t} \,\middle|\, \mathbf{x}_{\mathrm{u},t-1}, \mathbf{u}_t\right) \\ \mathrm{bel}\left(\mathbf{n}_{1:t-1}\right)\mathrm{bel}\left(\mathbf{x}_{\mathrm{u},0:t-1}\right),\end{aligned} \tag{11}$$

where $\eta$ is a normalizing constant given by the measurement prior. It will be sufficient to perform normalization to obtain $\eta$ as described in Section III-C. During the derivation, we used the assumption that the current measurement vector $\mathbf{z}_t$ is statistically independent of all previous system states $\mathbf{x}_{0:t-1}$ and data associations $\mathbf{n}_{0:t-1}$. Also, we assume a first order Hidden Markov Model (HMM), hence the current state $\mathbf{x}_{\mathrm{u},t}$ only depends on $\mathbf{x}_{\mathrm{u},t-1}$ and the current control signals $\mathbf{u}_t$. Similarly, the actual data association $\mathbf{n}_t$ only depends on the previous association $\mathbf{n}_{t-1}$. Following these assumptions, we obtain from (11) the belief in sequential form

$$\begin{aligned}\mathrm{bel}\left(\mathbf{x}_{\mathrm{u},0:t}\right) = \eta\mathrm{p}\left(\mathbf{x}_{\mathrm{u},0}\right)\prod_{i=1:t}\mathrm{p}\left(\mathbf{x}_{\mathrm{u},i} \,\middle|\, \mathbf{x}_{\mathrm{u},i-1}, \mathbf{u}_i\right) \\ \mathrm{p}\left(\mathbf{z}_i \,\middle|\, \mathbf{x}_{\mathrm{u},0:i}, \mathbf{z}_{1:i-1}\right),\end{aligned} \tag{12}$$

where the belief of the whole trajectory $\mathrm{bel}\left(\mathbf{x}_{\mathrm{u},0:t}\right)$ is obtained as a product of beliefs in all time steps.

Usually, we cannot calculate the most recent belief exactly, but according to [30] we can approximate the desired posterior PDF function by a posterior PMF composed of samples from a PDF with assigned weights

$$\mathrm{bel}\left(\mathbf{x}_{\mathrm{u},t}\right) \approx \sum_k w_t^{(k)}\delta\left(\mathbf{x}_{\mathrm{u},t} - \mathbf{x}_{\mathrm{u},t}^{(k)}\right), \tag{13}$$

where $\delta(\cdot)$ is a Dirac delta function. The weights $w_t^{(k)}$ can be obtained as a division of the target PDF and importance PDF as

$$w_t^{(k)} = \frac{\pi\left(\mathbf{x}_{\mathrm{u},t}^{(k)} \,\middle|\, \mathbf{z}_{1:t}, \mathbf{u}_{1:t}, \mathbf{n}_{1:t}\right)}{\mathrm{q}\left(\mathbf{x}_{\mathrm{u},t}^{(k)} \,\middle|\, \mathbf{z}_{1:t}, \mathbf{u}_{1:t}, \mathbf{n}_{1:t}\right)}, \tag{14}$$

where the nominator is the target PDF we desire to approximate by particles, and the denominator is the importance PDF the particles are sampled from.

Based on the Generic Particle Filter [30], our algorithm shows how to calculate the position and data association beliefs jointly. Using (11) as a target PDF, and

$$\underbrace{\mathrm{p}\left(\mathbf{z}_t \mid \mathbf{n}_t, \mathbf{x}_t\right)\overbrace{\mathrm{p}\left(\mathbf{n}_t \mid \mathbf{n}_{t-1}\right)}^{\text{MPC tracking}}}_{\text{Data association PDF}}\underbrace{\mathrm{p}\left(\mathbf{x}_{\mathrm{u},t} \,\middle|\, \mathbf{x}_{\mathrm{u},t-1}, \mathbf{u}_t\right)}_{\text{User state evolution PDF}} \tag{15}$$

as an importance PDF, the weight at time $t$ is proportional to

$$w_{t|t-1}^{(k)} = w_t^{(k)}w_{t-1|t-2}^{(k)}, \tag{16}$$

where we obtain the weights sequentially by setting

$$w_t^{(k)} \propto \mathrm{p}\left(\mathbf{z}_t \,\middle|\, \mathbf{x}_{\mathrm{u},t}^{(k)}, \mathbf{z}_{t-1}\right), \tag{17}$$

and

$$w_{t-1|t-2}^{(k)} \propto \text{bel}\left(\mathbf{n}_{1:t-1}\right) \text{bel}\left(\mathbf{x}_{\text{u},0:t-1}\right). \tag{18}$$

The likelihood in (17) can be interpreted as a marginal PDF over transmitters $\mathbf{x}_{\text{v},1:L\,t}$ and by directly using the independence between the individual MPCs and the product rule, the marginal PDF can be written as

$$\text{p}\left(\mathbf{z}_t \;\middle|\; \mathbf{x}_{\text{u},t}^{(k)}, \mathbf{z}_{t-1}\right) \propto \prod_{\ell} \int \text{p}\left(\mathbf{z}_t \;\middle|\; \mathbf{x}_{\text{u},t}^{(k)}, \mathbf{x}_{\text{v},\ell\,t}^{(k)}, \mathbf{z}_{t-1}\right) \text{p}\left(\mathbf{x}_{\text{v},\ell\,t}^{(k)} \;\middle|\; \mathbf{x}_{\text{u},t}^{(k)}, \mathbf{z}_{t-1}\right) \text{d}\mathbf{x}_{\text{v},\ell\,t}^{(k)}. \tag{19}$$

As in [19], we obtain from (19)

$$w_{t|t-1}^{(k)} \propto \prod_{\ell} \sum_{p} w_{\ell\,t-1|t-2}^{(k\,p)} \text{p}\left(\mathbf{z}_t \;\middle|\; \mathbf{x}_{\text{u},t}^{(k)}, \mathbf{x}_{\text{v},\ell\,t}^{(k\,p)}\right), \tag{20}$$

where the measurement likelihood function is calculated using samples approximating the transmitter position $\mathbf{x}_{\text{v},\ell\,t}^{(k\,p)}$ weighted by $w_{\ell\,t-1}^{(k\,p)}$ according to the multivariate PDF with a specified kernel function as in the regularized PF in [30].

### A. DATA ASSOCIATION

In the previous section, we derived a PF-based approximation of a position and data association joint belief. However, it must be stressed that this approximation only fits when we sample from the importance PDF defined by (15) where the last term is linked with the movement model and will be addressed in Section III-B. In this section, we focus on the first two terms, $\text{p}\left(\mathbf{z}_t \mid \mathbf{n}_t, \mathbf{x}_t\right)$, and $\text{p}\left(\mathbf{n}_t \mid \mathbf{n}_{t-1}\right)$, and propose a method to realize sampling from JPDF

$$\text{p}\left(\mathbf{z}_t \mid \mathbf{n}_t, \mathbf{x}_t\right) \text{p}\left(\mathbf{n}_t \mid \mathbf{n}_{t-1}\right). \tag{21}$$

The terminology used in this work is related to [21] where the reader can find a comprehensive description of the data association problematic, including practical examples. For the sake of thoroughness, we briefly define the terminology used in this section.

The measurement is assumed to be information provided by a detector when a detection condition is fulfilled. Thus, it is not the whole set of measured values, only its subset which fulfils certain conditions, e.g., the strength of the signal or the number of occurrences in the number of consecutive measurements ($m$-of-$n$). In our case, the KEST algorithm serves as a detector and tracker providing us with estimations of MPC parameters. We use measurement vector $\mathbf{z}_t$ defined in (8) as measurements.

However, even after being processed by the detector, some of the values in $\mathbf{z}_t$ can be caused by undesirable effects such as the thermal noise of the receiver, or interference with other systems operating in the same radio frequency band. Such values of $\mathbf{z}_t$ are called false alarms. As the detection is assumed only when such a value of $\mathbf{z}_t$ is provided by a detector and, at the same time, is not a false alarm. In other words, the detection is a measurement which is caused by the target. The target is observed as an MPC caused by an LoS signal, or a wall reflection, or a scatterer. The continuous observation of the target is called track. Finally, the set of false alarm measurements is called clutter.

The proposed algorithm assumes an unknown number of targets and is based on the MHT data association algorithm. The premise of the MHT is to assume data association as a random variable and to filter it using Bayesian filtration techniques. However, it requires an exhaustive search over the entire space of possible associations. The number of possible associations increases exponentially with an increasing number of targets which renders the MHT computationally infeasible in general. The derivation of the MHT can be found in [21]. Hence, we only outline the MHT algorithm derivation to demonstrate how our data association algorithm is similar to MHT, how the reduction of computational complexity is achieved, and how much it costs.

First, we define several statistics based on data association $\mathbf{n}_t$, which will be advantageous for further derivations:

- The track indicator

$$T_i = \begin{cases} 1; & \text{if } z_{i\,t} \text{ is caused by a tracked MPC} \\ 0; & \text{otherwise} \end{cases} \tag{22}$$

  is used to indicate that the $i$-th element of the measurement vector $z_{i\,t}$ originates from one of the already observed MPCs.
- The new target indicator

$$\nu_i = \begin{cases} 1; & \text{if } z_{i\,t} \text{ is caused by a new MPC} \\ 0; & \text{otherwise} \end{cases} \tag{23}$$

  indicates that $z_{i\,t}$ originates from a MPC which was not yet observed, and we need to establish a new track.
- The detection indicator

$$\delta_\ell = \begin{cases} 1; & \text{if } \mathbf{x}_{\text{v},\ell\,t} \text{ is detected at } t \\ 0; & \text{otherwise} \end{cases} \tag{24}$$

  provides us with information telling us whether the MPC linked with $\text{VT}_\ell$ is detected in current measurement vector $\mathbf{z}_t$.

Note that sums $T = \sum_i T_i$, and $\nu = \sum_i \nu_i$ provide the number of targets in $\mathbf{z}_t$. Then the number of false alarms is denoted by

$$\phi = |\mathbf{z}_t| - T - \nu. \tag{25}$$

To derive the data association posterior PDF of (10), we use the product rule and conditional independence to obtain

$$\text{p}\left(\mathbf{n}_{1:t} \mid \mathbf{x}_{0:t}, \mathbf{z}_{1:t}, \mathbf{u}_{1:t}\right) = \eta \text{p}\left(\mathbf{z}_t \mid \mathbf{n}_t, \mathbf{x}_t\right) \text{p}\left(\mathbf{n}_t \mid \mathbf{n}_{t-1}\right) \text{bel}\left(\mathbf{n}_{1:t-1}\right), \tag{26}$$

where we drop the independent variables assuming first order HMM. Notice also that we have ended with the exact same equation as association belief $\text{bel}\left(\mathbf{n}_{1:t}\right)$ from (11).

The first PDF on the right hand side (r.h.s.) of (26) is the likelihood function and can be evaluated using

indicators (22), (23), and (24) as

$$\mathrm{p}\left(\mathbf{z}_t \mid \mathbf{n}_t, \mathbf{x}_t\right) = V^{-\phi} \prod_{i=1}^{|\mathbf{z}_t|} \mathrm{p}\left(z_{i\,t}\right)^{\nu_i} \left[\mathrm{p}\left(z_{i\,t} \mid \mathbf{x}_{\mathrm{u},t}, \mathbf{x}_{\mathrm{v},n_{i\,t}\,t}\right)\right]^{T_i}, \tag{27}$$

where $n_{i\,t}$ is used to index the $\ell$-th VT. In cases when $z_{i\,t}$ is not associated with the $\ell$-th VT, the likelihood is given by a uniform PDF in a volume of interest $V$. Thus, for an unassociated element of $\mathbf{z}_t$, the likelihood is $V^{-1}$.

The likelihood of a newly established VT is given as a prior measurement given by $1/\sqrt{2\pi Q}$, where $Q$ is the measurement covariance. This idea can be intuitively viewed as the likelihood of a newly initialized transmitter $\mathbf{x}_{\mathrm{v},L+1\,t}$ since its prior state is generated to have zero residuals, as will be further addressed in the algorithm implementation section.

The second term $\mathrm{p}\left(\mathbf{n}_t \mid \mathbf{n}_{t-1}\right)$ in (26), which can be interpreted as the evolution of a data association state, is assumed to be independent of the previous step $\mathrm{p}\left(\mathbf{n}_t \mid \mathbf{n}_{t-1}\right) = \mathrm{p}\left(\mathbf{n}_t\right)$, when the KEST labels are not available. In this case, only the prior probability of data association $\mathrm{p}\left(\mathbf{n}_t\right)$ can be calculated.

When the data association algorithm obtains a measurement vector of cardinality $|\mathbf{z}_t|$, it needs to label each delay in $\mathbf{z}_t$ as either one of the previously observed VTs, or newly observed VT, or false alarm.

Each of the possible label assignments, how to assign $|\mathbf{z}_t|$ measurements with $|\mathbf{z}_t| - \phi$ VTs,[1] are equally probable. However, we need to calculate how many of these unique label assignments is possible to compose to calculate the value of $\mathrm{p}\left(\mathbf{n}_t\right)$.

Using the summed indicator functions $T$, $\nu$, and $\phi$, and the fact they are fully defined by $\mathbf{n}_t$, according to Section 6.3 [21] we can rewrite

$$\begin{aligned} \mathrm{p}\left(\mathbf{n}_t\right) &= \mathrm{p}\left(\mathbf{n}_t, T\left(\mathbf{n}_t\right), \nu\left(\mathbf{n}_t\right), \phi\left(\mathbf{n}_t\right)\right) \\ &= \mathrm{p}\left(\mathbf{n}_t \mid T\left(\mathbf{n}_t\right), \nu\left(\mathbf{n}_t\right), \phi\left(\mathbf{n}_t\right)\right) \\ &\quad \mathrm{p}\left(T\left(\mathbf{n}_t\right), \nu\left(\mathbf{n}_t\right), \phi\left(\mathbf{n}_t\right)\right), \end{aligned} \tag{28}$$

where the conditional term in (28) is calculated based on combinatorics. The number of possibilities of how to assign $|\mathbf{z}_t|$ measurements with $T$ previously observed targets is the number of permutations. The remaining possibilities are the combinations of how to label the remaining $\nu + \phi$ measurements as either a new track or a false alarm. Finally, the last term in (28) is modeled using clutter models.

However, since we have the KEST-based labels available, we can use

$$\mathrm{p}\left(\mathbf{n}_t \mid \mathbf{n}_{t-1}\right) \tag{29}$$

in our data association algorithm to greatly decrease the computational complexity. The idea is to use the label of the MPC provided by the KEST algorithm as a simple hard decision data association and use the soft decision data association algorithm only to resolve newly occurring MPCs, or re-occurring MPCs after the KEST outage. The KEST algorithm tracks the MPCs. However, individual MPCs might not always be visible. This causes some of the MPCs to disappear, or new MPCs to appear during the tracking. When a new MPC appears, the KEST algorithm initializes a new track and creates a unique label for this MPC. Since KEST does not assume re-tracking when a tracked MPC disappears, KEST removes such a track from its state. It also removes the associated label and never uses it again. We refer to removing the MPC from a KEST state as the KEST outage. The most common cause of the KEST outage is shadowing of the signal path or the signal propagation distance greater than the range of the transmitter. For details on how the KEST algorithm decides which MPC to remove, see [27].

It is not possible to use the MPC label directly as a data association for two reasons:

- After an outage in KEST the label of MPC is dropped and when the MPC originating from the same VT reappears, it is assigned a new label. Hence, we would be initializing a new VT despite the fact that the same VT has already been observed.
- Due to the "natural" data association used in KEST [27], the measurement can be assigned an incorrect KF causing an association error. Every error in KEST's association would cause a hard decision error leading to the divergence of the positioning algorithm.

Hence, we use the KEST-based association to shape the $\mathrm{p}\left(\mathbf{n}_t \mid \mathbf{n}_{t-1}\right)$, which would be otherwise independent of history $\mathbf{n}_{t-1}$ [21]. When the label of the $i$-th MPC provided by KEST is the same as the label which was previously linked with any of the VTs, we again link it with the same VT. This is assured by setting $\mathrm{p}\left(\mathbf{n}_t \mid \mathbf{n}_{t-1}\right) = 0$ otherwise. We illustrate this in an example: Vector $\mathbf{z}_{t-1}$ consists of three measurements with labels $L_{t-1} = [11, 22, 33]$. The measurements were assigned as VT two, three, and one; $\mathbf{n}_{t-1} = [2, 3, 1]$. In the following timestep, $\mathbf{z}_t$ consists of four measurements with $L_t = [11, 44, 55, 22]$. Since labels 11 and 22 were observed in the previous timestep and are still observed in the current timestep, we trust the KEST algorithm and set $n_{1\,t} = 2$, and $n_{4\,t} = 3$. The probability of any $\mathbf{n}_t$ violating the previous association is assumed zero. Hence, we do not need to calculate (26) for associations, where $n_{1\,t} \neq 2$ and $n_{4\,t} \neq 3$, which greatly reduces computational complexity.

Hence, using the KEST labels significantly decreases the number of possible $\mathbf{n}_t$ for which (26) needs to be calculated. Only the newly occurring labels need to be handled. At this moment we abandon the optimal approach because we are approximating the small probability that KEST is tracking an errant path by zero. For this reason, we additionally propose an algorithm resolving errors in the KEST labeling at the end of this section.

Finally, we can describe the algorithm used to associate the remaining unassociated measurements contained in a subset of $\mathbf{z}_t$, indicated by $\mathbf{z}'_t$, with the corresponding VTs. As shown in our PF derivation in Section III, we are able to perform

[1]Note that if the number of false alarms in measurement vector $\mathbf{z}_t$ is $\phi$ then the number of VTs in $\mathbf{z}_t$ is $|\mathbf{z}_t| - \phi$.

an estimation of joint PDF of the system state and data association by sampling from (15), hence we need to obtain samples from

$$\mathrm{p}\left(\mathbf{z}_t \mid \mathbf{n}_t, \mathbf{x}_t\right) \mathrm{p}\left(\mathbf{n}_t \mid \mathbf{n}_{t-1}\right). \tag{30}$$

Now, if we assume that all elements of $\mathbf{z}_t$ labeled with the same label as the previously observed VTs are already assigned together, then (30) will be proportional to

$$\mathrm{p}\left(\mathbf{z}'_t \mid \mathbf{n}'_t, \mathbf{x}'_t\right) \mathrm{p}\left(\mathbf{n}'_t\right), \tag{31}$$

where we have also omitted VTs associated with elements of $\mathbf{z}_t$ from $\mathbf{x}_t$ to obtain subsets marked by an apostrophe excluding already assigned data. Because of this, the remaining associations are independent of history and $\mathrm{p}\left(\mathbf{n}_t \mid \mathbf{n}_{t-1}\right)$, becomes an association prior $\mathrm{p}\left(\mathbf{n}'_t\right)$.

Essentially, the number of elements in $\mathbf{z}'_t$ is usually zero and only rarely is it greater than one. This means that, in most cases, data association is resolved solely by KEST. When we need to perform association according to (31), its complexity is, in most cases, reduced to assigning only one measurement with one of the set of currently unassigned VTs from $\mathbf{x}'_t$, with a new VT while creating $\mathbf{x}_{\mathrm{v},L+1\,t}$, or with a false alarm. However, when $\left|\mathbf{z}'_t\right| > 1$, we resolve elements of $\mathbf{z}'_t$ one after another which decreases the size of the space to search for each resolved element of $\mathbf{z}'_t$.

The optimal way would be to resolve all new occurrences jointly using the optimal MHT filter, but we have chosen the suboptimal method to decrease the computational complexity of the data association algorithm. Our method is to assign one measurement to one of the unassigned VTs, to a new VT, or to a false alarm. When more than one unassigned measurement is present, we apply the data association method for each measurement separately. The motivation for this is to limit the number of hypotheses under consideration. In other words, we obtain a subset of the most likely $\mathbf{n}_t$ for which we evaluate (26), while setting $\mathrm{p}\left(\mathbf{n}_t\right) = 0$ for all others $\mathbf{n}_t$. Since this approach is performed for each superordinate particle separately, we obtain a soft decision data association algorithm related to the MHT filter where the reduction of the number of hypotheses is also known as pruning [21].

Since we are associating a single element of $z'_{i\,t}$, the sampling from (31) is done as follows. First, we calculate

$$\mathrm{p}\left(z'_{i\,t} \mid n'_{i\,t}, \mathbf{x}'_t\right) \mathrm{p}\left(n'_{i\,t}\right) \tag{32}$$

for every possible value of $n'_{i\,t} = 1 : L'$, where $L'$ is the number of unassociated VTs. Then, we sample the desired number of particles from this PMF using a systematic resampling scheme [31]. Then we omit $z'_{i\,t}$ and $\mathbf{x}'_{\mathrm{v},n'_{i\,t}\,t}$ from $\mathbf{z}'_t$ and $\mathbf{x}'_t$. This process is repeated while $\left|\mathbf{z}'_t\right| > 0$.

To evaluate (32), we still need to show the solution for $\mathrm{p}\left(n'_{i\,t}\right)$. This solution can be found in [21] but, in our case, where we are not calculating associations jointly, we can model the prior as uniformly distributed for association with one of the older, currently unassociated VT. Then, the probability that the $z'_{i\,t}$ is a false alarm is given by a constant probability of false alarm $P_{\mathrm{FA}}$. Similarly, the PDF of a new target occurrence is the probability of new target $P_{\mathrm{N}}$. This can be written as

$$\mathrm{p}\left(n'_{i\,t}\right) = \begin{cases} P_{\mathrm{FA}}; & i = -1 \\ P_{\mathrm{N}}; & i = 0 \\ \dfrac{1 - P_{\mathrm{FA}} - P_{\mathrm{N}}}{\left|\mathbf{z}'_t\right|}; & \text{else.} \end{cases} \tag{33}$$

If we would like to perform data association jointly, we would need to model the false alarm and the new target occurrence as Poisson distributed random variables. Also, the number of possible associations would increase exponentially with the number of elements of $\mathbf{z}'_t$ rendering the joint data association into an extremely computationally demanding algorithm.

Finally, we address the situation where the KEST algorithm can make an incorrect data association. A KEST association error occurs when different targets cause almost identical observations. This situation typically occurs when the user is moving close to a wall, corners, or scatterer. Then the LoS delay is almost identical to the delay of MPC caused by the reflection from a nearby obstacle. This problem is especially severe if AoA information is not available. The algorithms e.g., [32], and [33] can resolve overlapping MPCs delays using AoA information. For these methods the data association provided by KEST labeling is sufficient, and the approximation used for KEST associated data, $\mathrm{p}\left(\mathbf{n}_t \mid \mathbf{n}_{t-1}\right) = 0$ is nearly true.

Unfortunately, the proposed algorithm uses low-cost hardware without AoA capability. Thus, we need to address this situation and suggest a solution to the KEST association error. We perform statistical testing to keep the associated track and discard the tracks with the probability of an association error

$$\mathrm{p}_{\mathrm{err}}^{(kp)} = 1 - \frac{1}{P\sqrt{2\pi Q}} \sum_{p=1}^{P} \mathrm{p}\left(\mathbf{z}_t \;\middle|\; \mathbf{x}_{\mathrm{u},t}^{(k)}, \mathbf{x}_{\mathrm{v},\ell\,t}^{(k\,p)}\right), \tag{34}$$

where $P$ is the number of particles used to approximate the $\ell$-th transmitter $\mathbf{x}_{\mathrm{v},\ell\,t}$, and $Q$ is the delay measurement covariance matrix. Note that this solution uses only the current time step likelihood since all track likelihood information is lost due to the weight normalization necessary in RBPF. This can result in a rather pessimistic value of error probability, but since we are performing MHT, we can decrease the number of discarded tracks using the power operation in the track discard condition

$$u < \left(\mathrm{p}_{\mathrm{err}}^{(kp)}\right)^{c_{\mathrm{err}}}; \quad u \sim \mathcal{U}\left(0, 1\right), \tag{35}$$

where $u$ is a number generated from a uniform distribution $\mathcal{U}\left(0, 1\right)$ on the interval from zero to one, and $c_{\mathrm{err}}$ is a constant providing the robustness of the algorithm without the necessity of increasing the number of particles.

### B. MOVEMENT MODEL

In this section, we derive a novel movement model for hand-held devices which incorporates IMU measurements.

Research in this area provides us with some models and techniques for using the acceleration measurement to improve position estimation. Plenty of transition models exist in the literature [20], [22], [34], [35], however they do not fit the application in question. Considering a hand-held device, it is not possible to double integrate body movement acceleration to calculate position because, while hand-holding, the pedestrian is accelerating the sensor in many directions which influences the measurement more than the actual pedestrian's movement. This problem is addressed, e.g., in [23], and [24] where step detection and step duration is used for positioning. This approach requires the creation of a step length estimator which can be done using a Bayesian framework and/or usually a nonlinear regression-based approximation of a feature function using, e.g., Support Vector Machine (SVM) or Artificial Neural Network (ANN).

In our approach, we utilize raw IMU measurements of angular velocities and accelerations, perform sensor calibration and extract yaw rate $\dot{\Psi}$, and the estimation of a Standard Deviation (STD) of acceleration $\beta$. The derivative of $\beta$, with respect to time, can be used to detect changes in walking style, especially if the pedestrian is standing still, increasing or decreasing the walking pace. Finally, the step frequency $\alpha$ based on a peak/valley step detector [24] is used with step length $\gamma$, to calculate the distance walked.

The novel idea presented in this work is that we can approximate not only position state vector $\mathbf{x}_{\mathrm{u},t}$ but also control signals $\mathbf{u}_t$, by a set of particles sampled from its prior. This idea allows us to incorporate IMU measurements directly into the movement model as stochastic control signals and better approximate the time evolution PDF. This idea presents a general approach allowing us to use a highly nonlinear movement model without linearization and approximation by Gaussian distributions. Moreover, since we are already using PF to calculate (11), the incorporation of $\mathbf{u}_t$ does not increase the computational complexity of the algorithm, while a better estimate of importance PDF greatly improves the performance of the whole positioning system.

The state vector is defined as

$$\mathbf{x}_{\mathrm{u},t} = \left[x_t, y_t, v_t, \Psi_t, b_{\dot{\Psi},t}, \gamma_t, b_{\mathrm{u},t}\right]^{\mathrm{T}}, \tag{36}$$

where $x_t$ and $y_t$ are coordinates of a receiver in a 2D Cartesian coordinate system, $v_t$ is the magnitude of a transmitter velocity vector in m/s, $\Psi_t$ is the yaw of a user in radians, $b_{\dot{\Psi},t}$ is a yaw rate bias in rad/s, $\gamma_t$ is a step length in meters, and the bias of a receiver clock after multiplying by the speed of light is in $b_{\mathrm{u},t}$.

The control signal vector is defined as

$$\mathbf{u}_t = \left[\dot{\Psi}_t, \alpha_t, \dot{\beta}_t, \xi_t, \varepsilon_t\right]^{\mathrm{T}}, \tag{37}$$

where $\dot{\Psi}_t$ is yaw rate in rad/s, $\alpha_t$ is the stepping frequency in Hz, $\dot{\beta}_t$ is a derivative of $\beta$ with respect to time, $\xi_t$ is a flag providing a binary estimation of whether the pedestrian is moving (1) or standing still (0). This *ismoving* flag is estimated according to the STD of accelerometer measurements. The last of the control signals, $\varepsilon_t$, is a flag indicating the validity of the control signals.

The state evolution step $\mathrm{p}\left(\mathbf{x}_{\mathrm{u},t} \mid \mathbf{x}_{\mathrm{u},t-1}, \mathbf{u}_t\right)$ is defined as a nonlinear vector function which is possible to separate into a set of equations, each corresponding to one variable from a state vector (36). The set of state equations is defined by (38)–(44).

The model used for position (38), (39), and velocity (40), as shown at the bottom of the next page is, essentially, the White Noise Acceleration (WNA) model [36] in 2D with the only difference being that velocity is modeled as a magnitude of velocity and angle in the direction of movement. In the beginning, the white noise samples for every particle are obtained from the Gaussian distributions with variances $\sigma^2_{w_x}$ and $\sigma^2_{w_y}$ for the $x$ and $y$ axes, respectively. Then, the generated values serve as a point-wise approximation of a Gaussian distribution. The variances are obtained from the expected dynamics of a system and sampling period using the relation

$$\Delta v \approx \sqrt{\delta_t \sigma^2_{w_x}}, \tag{45}$$

where $\Delta v$ is the maximal expected velocity difference between two measurements, and $\delta_t$ is the duration of a time step. Then, the expected covariance of a WNA model is obtained automatically because we are performing a simulation of this stochastic process using an approximation by particles.

Next, the velocity is calculated by two possible relations separated by validity flag $\varepsilon_t$ in (40). If the data provided by a step detector are not valid, then the term $(1 - \varepsilon_t) = 1$, and the future velocity is given by the previous velocity and the influence of random acceleration. The second case, when the pedometer data are valid, i.e., $\varepsilon_t = 1$, the future velocity is given by step length $\gamma_{t-1}$, step frequency $\alpha_t$, the *ismoving* flag $\xi_t$, and again by acceleration noise. Note that the measured values provided in the control signals are also represented as samples from their prior PDFs, similar to the acceleration noise in the movement model. This doubling of the velocity update equation allows us to predict the PDF of velocity even if the data provided by the IMU are not valid.

The prediction of yaw is given by (41), as shown at the bottom of the next page. It is based on a Micro-Electro-Mechanical System (MEMS) gyroscope measurement model using Angle Random Walk (ARW) and Bias Stability (BS) [37] to sample from its prior PDF. The ARW represents the STD of angle noise after the integration, usually in $^\circ/\sqrt{\mathrm{hr}}$. This value is provided by the manufacturer of the sensor. Then the prior PDF of the angular velocity measurement $\dot{\Psi}_t$ in (41) is given by

$$\dot{\Psi}_t = \breve{\dot{\Psi}}_t + \frac{\pi}{180\sqrt{3600}} \frac{1}{\sqrt{\delta_t}} \mathcal{N}\left(0, \sigma^2_{\mathrm{ARW}}\right), \tag{46}$$

where the $\breve{\dot{\Psi}}_t$ is the measured yaw rate value in rad/s obtained from a gyroscope after the sensor calibration. The check symbol $\breve{}$ is used to mark values provided by the IMU after calibration. The BS, the second parameter of the gyroscope

measurement model, is included in a yaw rate bias estimator in (42), as shown at the bottom of the this page. If we assume that the calibration took place at the beginning of a measurement, we can also assume that the calibrated bias of a yaw rate is a zero-mean random number with Gaussian distribution and the STD $\sigma_{\mathrm{BS}}$ in rad/s.

The estimation of step length is provided in (43), as shown at the bottom of the this page, where the prediction of the step length in the following time step is modeled as a random variable given by the old value $\gamma_{t-1}$, and Gaussian zero mean distributed noise with the STD $\sqrt{\delta_t}\sigma_\gamma$. The last part of the step update equation is linked with the IMU measurement and walking pace estimation [24] where $\dot{\beta}_t$ is obtained as

$$\dot{\beta}_t = \breve{\dot{\beta}}_t + \delta_t \mathcal{N}\left(0, \sigma_{\ddot{\beta}}^2\right), \tag{47}$$

where $\sigma_{\ddot{\beta}}$ is chosen high enough to cover the errors of $\breve{\dot{\beta}}_t$, which is the estimated derivative of $\breve{\beta}_t$ provided by the step counting algorithm as

$$\breve{\dot{\beta}}_t = \frac{\breve{\beta}_t - \breve{\beta}_{t-1}}{\delta_t}, \tag{48}$$

where function $\breve{\beta}_t$ is an estimation of the acceleration STD obtained by filtering the measured acceleration by a low pass Butterworth filter.

We model the change of step length in (43) as a value proportional to the change of acceleration STD with proportionality constant $c_\beta$. This simplification, of an unknown dependence between the accelerometer measurement and the actual change of the step length, is possible when we assume a random distribution of the error of such mapping, as shown in (47).

Finally, the time bias of a receiver is predicted by (44), as shown at the bottom of the this page. The receiver bias is modeled as a Wiener process with an STD $\sqrt{\delta_t}\sigma_{\mathrm{Rx}}$.

The velocity update (40) used information extracted from the IMU measurement but its PDFs had not yet been provided. The measured step frequency $\alpha_t$ is a Gaussian distributed random number defined as

$$\alpha_t = \breve{\alpha}_t + \mathcal{N}\left(0, \sigma_\alpha^2\right), \tag{49}$$

where $\breve{\alpha}_t$ is a step frequency value provided by the step counter algorithm.

The PMF of a validity flag is binomial because there is a nonzero probability that an error in a step detector algorithm was made and the flag should be inverted with probability $\mathrm{p}_\varepsilon$. Then this PMF can be expressed as

$$\varepsilon_t = \|\left(u < \mathrm{p}_\varepsilon\right) - \breve{\varepsilon}_t\|; \quad u \sim \mathcal{U}\left(0, 1\right), \tag{50}$$

where $\breve{\varepsilon}$ is the validity flag provided by the step counting algorithm and $u$ is a uniformly distributed random number on the interval from zero to one.

Finally, the *ismoving* flag PMF is obtained as

$$\xi_t = \|\left(u < \mathrm{p}_\zeta\right) - \breve{\zeta}_t\| \,\Big|\Big|\, \left(!\varepsilon_t\right); \quad u \sim \mathcal{U}\left(0, 1\right), \tag{51}$$

where $\breve{\zeta}_t$ is a moving condition flag provided by the step counter algorithm, $\Big|\Big|$ is logical *or* operator, and ! is logical *not* operator. $\breve{\zeta}_t$ is equal to one if the actual set of peaks and valleys detected in the measured acceleration was in the process of forming a sequence peak-zero-valley which was then evaluated as a valid step. However, the $\breve{\zeta}_t$ flag is not valid when the user is standing still. For this reason $\xi_t$ is given as a binomial distribution of $\breve{\zeta}$ with a probability of error $\mathrm{p}_\zeta$ only

$$x_t = x_{t-1} + \delta_t v_{t-1}\cos\left(\Psi_{t-1} + \delta_t\left(\dot{\Psi}_t + b_{\dot{\Psi},t-1}\right)\right) + \sqrt{\frac{\delta_t^3}{3}}\mathcal{N}\left(0, \sigma_{w_x}^2\right), \tag{38}$$

$$y_t = y_{t-1} + \delta_t v_{t-1}\sin\left(\Psi_{t-1} + \delta_t\left(\dot{\Psi}_t + b_{\dot{\Psi},t-1}\right)\right) + \sqrt{\frac{\delta_t^3}{3}}\mathcal{N}\left(0, \sigma_{w_y}^2\right), \tag{39}$$

$$\begin{aligned} v_t = {} & (1-\varepsilon_t)\sqrt{\left[v_{t-1}\cos\left(\Psi_{t-1} + \delta_t\left(\dot{\Psi}_t + b_{\dot{\Psi},t-1}\right)\right) + \sqrt{\delta_t}\mathcal{N}\left(0, \sigma_{w_x}^2\right)\right]^2} \\ & + \left[v_{t-1}\sin\left(\Psi_{t-1} + \delta_t\left(\dot{\Psi}_t + b_{\dot{\Psi},t-1}\right)\right) + \sqrt{\delta_t}\mathcal{N}\left(0, \sigma_{w_y}^2\right)\right]^2} \\ & + \varepsilon_t\sqrt{\left[\xi_t\alpha_t\gamma_{t-1}\cos\left(\Psi_{t-1} + \delta_t\left(\dot{\Psi}_t + b_{\dot{\Psi},t-1}\right)\right) + \sqrt{\delta_t}\mathcal{N}\left(0, \sigma_{w_x}^2\right)\right]^2} \\ & + \left[\xi_t\alpha_t\gamma_{t-1}\sin\left(\Psi_{t-1} + \delta_t\left(\dot{\Psi}_t + b_{\dot{\Psi},t-1}\right)\right) + \sqrt{\delta_t}\mathcal{N}\left(0, \sigma_{w_y}^2\right)\right]^2}, \end{aligned} \tag{40}$$

$$\Psi_t = \Psi_{t-1} + \delta_t\left(\dot{\Psi}_t + b_{\dot{\Psi},t-1}\right), \tag{41}$$

$$b_{\dot{\Psi},t} = b_{\dot{\Psi},t-1} + \mathcal{N}\left(0, \sigma_{\mathrm{BS}}^2\right), \tag{42}$$

$$\gamma_t = \gamma_{t-1} + c_\beta\delta_t\dot{\beta}_t + \sqrt{\delta_t}\mathcal{N}\left(0, \sigma_\gamma^2\right), \tag{43}$$

$$b_{\mathrm{u},t} = b_{\mathrm{u},t-1} + \sqrt{\delta_t}\mathcal{N}\left(0, \sigma_{\mathrm{Rx}}^2\right). \tag{44}$$

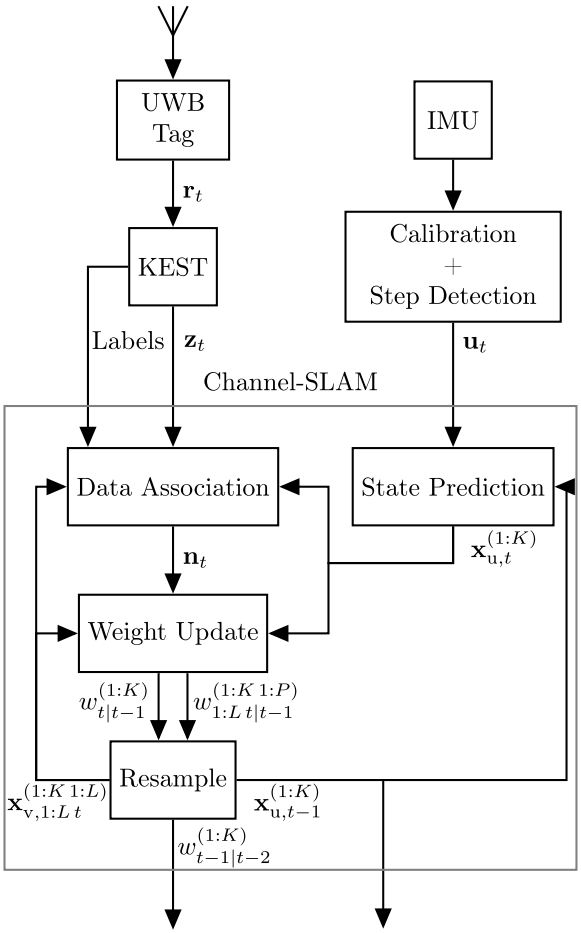


**FIGURE 3.** Block diagram of the proposed multipath assisted positioning algorithm.

when the control signal is valid ($\varepsilon_t = 1$). The *ismoving* flag is raised otherwise.

### C. IMPLEMENTATION OF THE POSITIONING ALGORITHM

This section aims to address practical problems which need to be solved for the implementation of the proposed Channel-SLAM algorithm. Also, we show the pseudocode of a proposed implementation in Algorithm 1, and the pseudocode for a proposed data association method in Algorithm 2. The principle of the algorithm is illustrated by Fig. 3.

Algorithm 1 describes the proposed Channel-SLAM implementation running from initial time $T_{\mathrm{beg}}$ given by time index $t = 1$ up to time $T_{\mathrm{end}}$ given by time index $t_{\mathrm{end}}$. The initial set of $K$ particles is drawn from a prior PDF $\mathrm{p}\left(\mathbf{x}_{\mathrm{u},0}\right)$. The gyroscope offset $b_{\dot{\Psi},0}$ is set to zero because we calibrate the IMU sensor at the beginning of a measurement. The initial step length $\gamma_0$ is normally distributed with a mean value corresponding to the walk of an average person. The initial receiver time bias $b_{\mathrm{u},0}$ is assumed to be normally distributed with a zero mean.

After the initialization of the user state, the *while* loop in Algorithm 1 Line 2 is entered. The user state is predicted in Line 4 using the derived movement model described by (38)–(44). If the measurement vector $\mathbf{z}_t$ is not an empty vector, we enter the *for* loop performing the data association in Lines 6–15 as described in Section III-A. The weight calculation described in Section III is applied to Lines 17–23. Finally, the resampling in Lines 26 and 32 is performed using a systematic resampling scheme [31]. This *for* loop is executed for all of the user particles independently.

The steps of data association in Algorithm 1 proceed as follows:

- The MPC labels provided by KEST are associated with VTs with the same label.
- The remaining unresolved measurements $\mathbf{z}'_t$ are handed over to the data association routine Algorithm 2 which associate $z'_{it}$ with:
  - False alarm if $n_{jt}^{(k)} < 0$.
  - A new $\mathrm{VT}_{L+1}$ which will be initialized if $n_{jt}^{(k)} = 0$.
  - $\mathbf{x}_{\mathrm{v},n_{jt}^{(k)}\,t}^{(k\,1:P)}$ if $n_{jt}^{(k)} > 0$.

This routine is done independently for each of the user state particles. If any of the elements in $\mathbf{z}'_t$ are labeled as a false alarm, it will be omitted from $\mathbf{z}_t$ for the corresponding user state particle.

The initial state of a $p$-th particle of an $\ell$-th virtual transmitter $\mathbf{x}_{\mathrm{v},\ell\,t}^{(k\,p)}$ is obtained by sampling a position uniformly distributed inside the radius $r = z'_{it} + 3\sqrt{Q}$ with the center in $\mathbf{x}_{\mathrm{u},t}^{(k)}$ to assure that the true propagation distance is lower than $r$ with a probability higher than 99.7 %. The additional propagation length $b_{\mathrm{v},\ell\,t}^{(k\,p)}$ is sampled as a normally distributed variable with covariance $Q$ and the mean value calculated as

$$\mu_{b_{\mathrm{v},\ell\,t}^{(k\,p)}} = z'_{it} - \|\mathbf{x}_{\mathrm{Rx},t}^{(k)}, \mathbf{x}_{\mathrm{Tx},\ell\,t}^{(k\,p)}\| - b_{\mathrm{u},t}^{(k)}, \tag{52}$$

to support the existence of scatterers. The norm $\|\mathbf{x}_{\mathrm{Rx},t}^{(k)}, \mathbf{x}_{\mathrm{Tx},\ell\,t}^{(k\,p)}\|$ denotes a physical distance between the user and virtual transmitter position in Cartesian coordinates. The act of sampling the values of $b_{\mathrm{v},\ell\,t}^{(k\,p)}$ from a normal distribution assures the independence of the VT prior PDF and the concrete realization of $z'_{it}$. Thus, the influence of the distance measurement error is marginalized when initializing the VT, assuming $b_{\mathrm{v},\ell\,t}^{(k\,p)}$ to be a random variable. The number of particles necessary to initialize the transmitter state can be obtained from Gauss's circle problem [38]. If a new transmitter is initialized, we initialize the set of initial weights as

$$w_{n_{it}^{k}\,t-1|t-2}^{(kp)} = 1/\sqrt{2\pi Q}. \tag{53}$$

Now, when all elements of $\mathbf{z}_t$ are either associated with a transmitter or treated as a false alarm, we can proceed to the weight calculation step. The weights of virtual transmitter particles are calculated in Algorithm 1 Line 17. The likelihood function is evaluated assuming a normal distribution of

a $z_{it}$ error with covariance $Q$ as

$$w^{(k\,p)}_{n^{(k)}_{it}\,t} = \frac{1}{\sqrt{2\pi Q}} \mathrm{e}^{-\frac{\left(z_{it} - \|\mathbf{x}^{(k)}_{\mathrm{Rx},t}, \mathbf{x}^{(k\,p)}_{\mathrm{Tx},\ell\,t}\| - b^{(k)}_{\mathrm{u},t} - b^{(k\,p)}_{\mathrm{v},n^{(k)}_{it}\,t}\right)^2}{2Q}}. \quad (54)$$

The main problem is the fact that we are not able to normalize weights associated with virtual transmitters, i.e., to sum up to the unit, because in that case the differences between the likelihoods of individual VTs would be lost. The next idea might be to omit the normalization for weight calculation and normalize it only for the resampling step. However, in this case, we would face a numerical instability problem, since the weights are always lower than one if covariance $Q > 1/(2\pi)$ and, thus, all weights would geometrically converge to zero. The multiplication in (16) causes this vanishing of weights.

We solve the weight normalization problem using a forgetting scheme given in Algorithm 1 Line 18. Details on forgetting, in approximate Bayesian filtering, can be found in [39]–[41], and [42] where the forgetting is used for RBPF. The motivation for our square root forgetting is to ensure numerical stability for high $Q$ while preserving properties of the individual virtual transmitters and how strongly it should influence the user position weights calculated in Algorithm 1 Line 22.

If the KEST algorithm associates one or more MPCs with a wrong label it would cause an incorrect association of one or more elements in $\mathbf{z}_t$ with VTs resulting in the corruption of position estimation, and since we trust the provided labels as described in Section III-A, we would not be able to recover from it by resampling. The proposed solution enables the provided labels with a probability proportional to the likelihood of the VT to be forgotten. The VTs with a lower likelihood have a higher probability that an incorrect association will occur. This step is done in Algorithm 1 Line 20.

At the end of this section, we mention that the number of virtual transmitter state particles $P$ is not fixed and decreases as the estimated variance of a transmitter position decreases. This concept allows us to save memory and computational resources while the algorithm precision remains unchanged. To implement this, the mean and variance of a user and a transmitter state must be estimated. Note that the estimation of the first two moments does not provide complete information, but we use them to estimate characteristics as a Root-Mean-Square Error (RMSE) of the position estimation, and the required number of particles to sufficiently approximate the state of the VTs. The estimation of the expected value in PF is straightforward. Since the weights assigned to particles represent the PMF approximation of the PDF, the expected value of the user state is approximated as

$$\hat{\mu}_{\mathbf{x}_{\mathrm{u},t}} = \frac{1}{\sum_k w^{(k)}_{t|t-1}} \sum_k w^{(k)}_{t|t-1} \mathbf{x}^{(k)}_{\mathrm{u},t}. \quad (55)$$

The estimation of a VT expected state is done in two steps as

$$\hat{\mu}_{\mathbf{x}^{(k)}_{\mathrm{v},\ell\,t}} = \frac{1}{\sum_p w^{(k\,p)}_{\ell\,t|t-1}} \sum_p w^{(k\,p)}_{\ell\,t|t-1} \mathbf{x}^{(k\,p)}_{\mathrm{v},\ell\,t}, \quad (56)$$

$$\hat{\mu}_{\mathbf{x}_{\mathrm{v},\ell\,t}} = \frac{1}{\sum_k w^{(k)}_{t|t-1}} \sum_k w^{(k)}_{t|t-1} \hat{\mu}_{\mathbf{x}^{(k)}_{\mathrm{v},\ell\,t}}, \quad (57)$$

to allow the dynamic number of the particles for each of the subordinate PFs separately. The VT's expected state estimation is used to estimate its second central moment

$$\hat{\sigma}^2_{\mathbf{x}^{(k)}_{\mathrm{v},\ell\,t}} = \frac{1}{\sum_p w^{(k\,p)}_{\ell\,t|t-1}} \sum_p w^{(k\,p)}_{\ell\,t|t-1} \left(\mathbf{x}^{(k\,p)}_{\mathrm{v},\ell\,t} - \hat{\mu}_{\mathbf{x}^{(k)}_{\mathrm{v},\ell\,t}}\right)^2, \quad (58)$$

$$\hat{\sigma}^2_{\mathbf{x}_{\mathrm{v},\ell\,t}} = \frac{1}{\sum_k w^{(k)}_{t|t-1}} \sum_k w^{(k)}_{t|t-1} \hat{\sigma}^2_{\mathbf{x}^{(k)}_{\mathrm{v},\ell\,t}}. \quad (59)$$

The number of particles in subordinate PF is proportional to

$$P = c_P \sqrt{\sum \left(\hat{\sigma}^2_{\mathbf{x}^{(k)}_{\mathrm{Tx},\ell\,t}}\right)}, \quad (60)$$

with a proportionality constant $c_P$. The summation is performed over the dimensions of a VT's position $\mathbf{x}^{(k)}_{\mathrm{Tx},\ell\,t}$.

## IV. EVALUATION OF THE PROPOSED ALGORITHM PRECISION

### A. MEASUREMENT ENVIRONMENT AND EQUIPMENT

The measurements were conducted using a UWB system based on the *Decawave DWM1000* chip using a two-way-ranging method, see e.g., [43]. The precision of the *Decawave DWM1000* Time of Arrival (ToA) estimation is 10 cm. The measurement setup consists of one static UWB anchor and a hand-held device carried by a walking pedestrian. The hand-held device includes a UWB tag, an Xsense IMU (MTI-G-700) and a laptop which stores the IMU and UWB measurement data. For the measurements, the UWB system is configured to a bandwidth of [500] MHz and a carrier frequency of [3.5] GHz. The *Decawave DWM1000* chip can provide, in addition to the ranging information, the measured CIR.

The measurement was performed in a rectangular room with support pillars on one side. Two different volunteers performed the experiment. Both volunteers were changing speed and completely stopped, at least once for a short period during the walk. The duration of each experiment was 140 seconds. Fig. 4 shows the environment layout, the ground truth of the pedestrian movement, the UWB anchor position indicated by $\mathrm{VT}_1$, and the VT positions $\mathrm{VT}_2$–$\mathrm{VT}_6$.

We used a Vicon motion capturer to track the movement of the pedestrians, hence, to obtain the ground truth of the pedestrian movement. The Vicon motion capture system is capable of tracking the motion of the Vicon reflective marker in a room with a ground area of approximately 7 m by 4 m within an accuracy below 1 cm. The Vicon reflective

**Algorithm 1** Channel-SLAM

Initialize $K$ particles from PDF $\mathrm{p}\left(\mathbf{x}_{\mathrm{u},t=0}\right)$; $t=1$;
**while** $t < t_{\mathrm{end}}$
  **for** $k = 1:K$
    $\mathbf{x}_{\mathrm{u},t}^{(k)} = \mathit{UpdateState}\left(\mathbf{x}_{\mathrm{u},t-1}^{(k)}, \mathbf{u}_t^{(k)}\right)$ // see (38)–(44)
  **if** $\mathbf{z}_t \neq \emptyset$
    **for** $k = 1:K$
      Associate using KEST labels // see (29)
      **if** $\mathbf{z}'_t \neq \emptyset$
        **for** $i = 1:|\mathbf{z}'_t|$
          $j = \mathrm{argmax}\left(\mathbf{z}_t == z'_{it}\right)$
          // Associate $z'_{it}$ using Algorithm 2
          $n_{jt}^{(k)} = \mathit{Associate}\left(z'_{it}, \mathbf{x}_{\mathrm{u},t}^{(k)}, \mathbf{x}_{\mathrm{v},1:L\,t}^{(k\,1:P)}, \mathbf{n}_t^{(k)}, Q_i\right)$
          **if** $n_{jt}^{(k)} == -1$
            Omit $z'_{jt}$ from $\mathbf{z}_t$
          **else if** $n_{jt}^{(k)} == 0$
            // Section III-C
            Initialize $\mathbf{x}_{\mathrm{v},L+1\,t}^{(k\,1:P)}$ using $\mathbf{x}_{\mathrm{u},t}^{(k)}$
      **for** $i = 1:|\mathbf{z}_t|$
        $w_{n_{it}^{(k)}\,t}^{(k\,p)} = \mathit{evalLikelihood}\left(z_{it}, \mathbf{x}_{\mathrm{u},t}^{(k)}, \mathbf{x}_{\mathrm{v},n_{it}^{(k)}\,t}^{(k\,p)}\right)$ // see (54)
        $w_{n_{it}^{(k)}\,t|t-1}^{(k\,p)} = \sqrt{w_{n_{it}^{(k)}\,t-1|t-2}^{(k\,p)}\, w_{n_{it}^{(k)}\,t}^{(k\,p)}}$
        $u = \mathrm{rand}\,(0,1)$
        **if** $u < \left(1 - \frac{1}{P\sqrt{2\pi Q}} \sum_{p=1}^{P} w_{n_{it}^{(k)}\,t|t-1}^{(k\,p)}\right)^{c\mathrm{err}}$ // see (34)
          Remove $\mathbf{x}_{\mathrm{v},n_{it}^{(k)}\,t}^{(k\,1:P)}, n_{it}^{(k)}$ from $\mathbf{x}_{\mathrm{v},1:L\,t}^{(k\,1:P)}, \mathbf{n}_t^{(k)}$
      $w_{t|t-1}^{(k)} = \prod_{\ell=1}^{|\mathbf{z}_t|} \frac{1}{P} \sum_{p=1}^{P} w_{\ell\,t|t-1}^{(k\,p)}$ // see (20)
  $w_{t|t-1}^{(1:K)} = w_{t|t-1}^{(1:K)} \left(\sum_{k=1}^{K} w_{t|t-1}^{(k)}\right)^{-1}$
  // superordinate PF resampling
  $n_{\mathrm{Eff}}^{-1} = K \sum_{k=1}^{K} \left(w_{t|t-1}^{(k)}\right)^2$
  **if** $n_{\mathrm{Eff}} < n_{\mathrm{SupPF}}$
    $\mathit{resampleSR}\left(\left[\mathbf{x}_{\mathrm{u},t}^{(1:K)}, \mathbf{x}_{\mathrm{v},1:L\,t}^{(1:K\,1:P)}\right], w_{t|t-1}^{(1:K)}, K\right)$ // see [31]
    $w_{t|t-1}^{(1:K)} = \frac{1}{K}$
  // subordinate PF resampling
  **for** $k = 1:K$
    **for** $i = 1:|\mathbf{z}_t|$
      $n_{\mathrm{Eff}}^{-1} = P \sum_{p} \left(w_{n_{it}^{(k)}\,t|t-1}^{(k\,p)}\right)^2$
      **if** $n_{\mathrm{Eff}} < n_{\mathrm{SubPF}}$
        $\mathit{resampleSR}\left(\mathbf{x}_{\mathrm{v},n_{it}^{(k)}\,t}^{(k\,1:P)}, w_{n_{it}^{(k)}\,t|t-1}^{(k\,1:P)}, P_{\mathrm{new}}\right)$ // see [31]
        $w_{n_{it}^{(k)}\,t|t-1}^{(k\,1:P)} = 1/\sqrt{2\pi Q}$
  $w_{1:L\,t-1|t-2}^{(1:K\,1:P)} = w_{1:L\,t|t-1}^{(1:K\,1:P)}$; $t = t+1$;

**Algorithm 2** Data Association

**Input**: $z_{i\,t}, \mathbf{x}_{\mathrm{u},t}^{(k)}, \mathbf{x}_{\mathrm{v},1:L\,t}^{(k\,1:P)}, \mathbf{n}_t^{(k)}, Q$
**Output**: $n$
**for** $\ell = -1:L$
  **if** $\ell == -1$
    $p_\ell = P_{\mathrm{FA}}$
  **else if** $\ell == 0$
    $p_\ell = P_{\mathrm{N}}/\sqrt{2\pi Q}$
  **else if** $n_{\ell\,t}^{(k)} == 0$
    $p_\ell = \frac{1-P_{\mathrm{N}}}{P} \sum_{p=1}^{P} \mathit{evalLikelihood}\left(z_{i\,t}, \mathbf{x}_{\mathrm{u},t}, \mathbf{x}_{\mathrm{v},\ell\,t}^{(k\,1:P)}\right)$ // see (54)
$\eta^{-1} = \sum_{\ell=0}^{L} p_\ell$
**for** $\ell = 0:L$
  $p_\ell = \eta p_\ell\,(1 - P_{\mathrm{FA}})$
$n = \{-1; 0; \ldots; L\}$
$n = \mathit{resampleSR}(n, p, 1)$ // see [31]

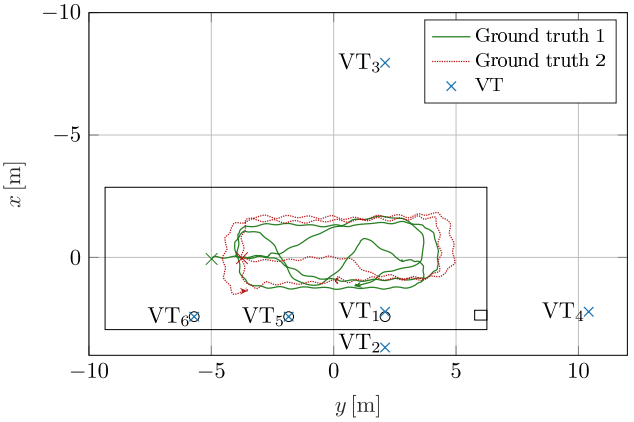


**FIGURE 4.** The environment layout with the ground truth of the pedestrian movement during the performed experiments. The cross and arrow mark the beginning and end of the experimental trajectory, respectively. The blue crosses mark the positions of six virtual transmitters. $\mathbf{VT_1}$ is the position of the physical transmitter. $\mathbf{VT_2}$–$\mathbf{VT_4}$ are caused by the reflections from the room walls. $\mathbf{VT_5}$–$\mathbf{VT_6}$ are caused by the scattering of the transmitted signal on the room support pillars.

marker which was tracked by the Vicon motion capturer, was attached to the hand-held device.

During the experiment, the ground truth of the pedestrian movement, the IMU measurements, and the CIR provided by the target UWB anchor were captured online while the pedestrian was walking. The positioning was carried out offline using the collected data.

### B. EVALUATIONS OF PRECISION BASED ON A SIMULATION

The simulation is performed to show the performance of the proposed algorithms. Hence, the simulation assumes one physical transmitter, three wall reflections, and two scatterers. Based on the geometry, the positions of the VTs can be obtained as described in II-B. The measurement vector $\mathbf{z}_{1:t}$

**TABLE 1. Parameters used for the evaluation of the simulations.**

| | | | |
|---|---|---|---|
| $K$ | 2000 | $c_P$ | 1000 |
| $Q$ | $0.36\,\mathrm{m}^2$ | $\sigma_{w_x}$ | $0.15\,\mathrm{m/s}^{3/2}$ |
| $\sigma_{w_y}$ | $0.15\,\mathrm{m/s}^{3/2}$ | $\sigma_{\mathrm{BS}}$ | $10\,\mathrm{deg/h}$ |
| $\sigma_\gamma$ | $5\cdot10^{-3}\,\mathrm{m/s}^{3/2}$ | $\sigma_{\mathrm{Rx}}$ | $1\cdot10^{-3}\,\mathrm{m/s}^{1/2}$ |
| $\sigma_{\mathrm{ARW}}$ | $10\,^\circ/\sqrt{\mathrm{hr}}$ | $\sigma_{\ddot{\beta}}$ | $1\cdot10^{-4}\,\mathrm{m/s}^4$ |
| $\sigma_\alpha$ | $1\cdot10^{-4}\,\mathrm{Hz}$ | $\mathrm{p}_\varepsilon$ | $1\cdot10^{-3}$ |
| $\mathrm{p}_\zeta$ | $1\cdot10^{-3}$ | $c_{\mathrm{err}}$ | 3.8 |

is simulated as a noisy signal propagation distance between the VT and the ground truth position $\mathbf{x}^{\mathrm{GT}}_{\mathrm{u},1:t}$ including the additional propagation length $b_{\mathrm{v},t}$ for scatterers $\mathrm{VT}_5$–$\mathrm{VT}_6$. The assumed noise of $\mathbf{z}_{1:t}$ is normally distributed with STD $\sigma = 0.1$ m, corresponding to the precision of the UWB system based on the *Decawave DWM1000* chip.

As with the real experiment, we assume outages in the MPCs observations in the simulation. Similarly, in an actual KEST-based estimation, the simulator generates a new KEST label after an outage. The probability of the MPC outage is selected for each MPC separately to achieve visibility for a desired percentage of the time. When an outage occurs, the outage duration is generated as a uniformly distributed random number between zero and 10 seconds $\mathcal{U}(0, 10)$. The percentage of visibility was selected 0.8, 0.7, 0.6, 0.5, 0.4, and 0.3 for $\mathrm{MPC}_1$–$\mathrm{MPC}_6$ respectively.

The movement model uses the recorded IMU measurements as input because creating an IMU measurement simulator for a walking pedestrian is not part of this work. The IMU measurements serve as control signals for the movement model, see Section III-B. The trajectory recorded by the Vicon motion capturer was used as a ground truth of the pedestrian movement $\mathbf{x}^{\mathrm{GT}}_{\mathrm{u},1:t}$ for the simulation of $\mathbf{z}_{1:t}$, and for the precision evaluation. By this approach, we show the performance of the proposed Channel-SLAM algorithm, including the data association, compared to the state-of-the-art approach presented in [20].

Table 1 summarizes the values of the parameters used in the simulation. The parameters of the movement model are set to fit all the measured scenarios.

The STD of the *Decawave DWM1000* chip ToA estimation is 10 cm. However, the STD of the MPC delay estimate is higher due to a low SNR of the reflections. We set the MPC variance $Q = 0.36\,\mathrm{m}^2$ for our experiments. Therefore, we use the same value for simulations.

The bias stability of the Xsense IMU (MTI-G-700) gyroscope is $10°/\mathrm{h}$, which is directly used as the movement model parameter $\sigma_{\mathrm{BS}}$. Similarly, the noise density of the IMU gyroscope is $0.01°/\mathrm{s}/\sqrt{\mathrm{Hz}}$, which corresponds to the angular random walk $6°/\mathrm{h}$ when a 100 Hz bandwidth is assumed. The parameter tuning showed that the increased value $\sigma_{\mathrm{ARW}} = 10\,^\circ/\sqrt{\mathrm{hr}}$ yields better performance.

The parameters influencing the pedestrian velocity ($\sigma_{w_x}$, $\sigma_{w_y}$, $\sigma_\gamma$, $\sigma_{\ddot{\beta}}$, and $\sigma_\alpha$) are set to envelope the walking dynamics similar to the WNA model [36]. However, when the choice is too large, the deviation of the superordinate particles is also large, resulting in a high number modes of the estimated posterior PDF, which significantly decreases the precision.

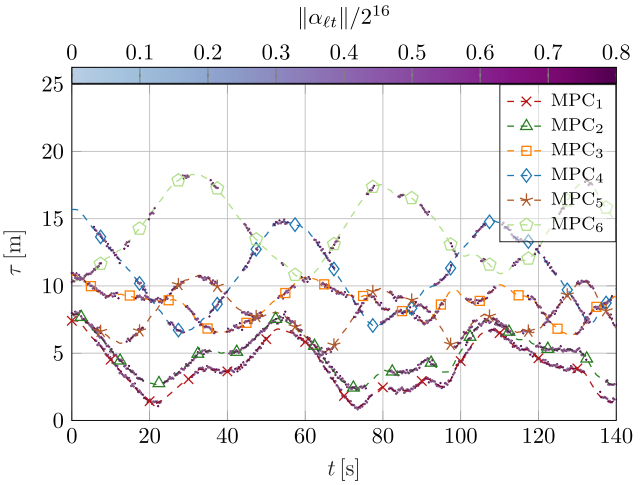


**FIGURE 5. The simulated CIR with ground true MPCs for the scenario number one. The MPC outage is designed to achieve the time percentage of visibility 0.8, 0.7, 0.6, 0.5, 0.4, and 0.3 for $\mathrm{MPC}_1$–$\mathrm{MPC}_6$, respectively. The magnitude of the estimated impulse response $\|\alpha_{\ell t}\|$ is not assumed in the simulation.**

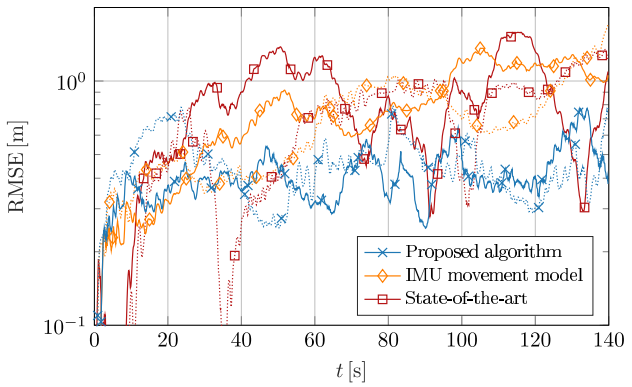


**FIGURE 6. Comparison of the simulated RMSE of the proposed Channel-SLAM algorithm and the state-of-the-art Channel-SLAM [20]. The achieved precision of the IMU-based movement model without using the Channel-SLAM is shown by the orange line. The solid and dotted lines illustrate the first and the second scenarios, respectively.**

Fig. 5 shows an example of the simulated CIRs for recorded scenario number one. The random outages of the noisy MPC observations provide a short time track similar to a real MPC parameter estimation provided by KEST. Since the amplitude of the MPC is not included in the proposed Channel-SLAM, we simplify the simulation by setting a constant amplitude for all MPCs.

Fig. 6 compares the performance of the proposed Channel-SLAM algorithm with the state-of-the-art approach [20] for each simulation. The solid and dotted lines illustrate the first and second scenarios, respectively. The RMSE of the proposed algorithm never exceeds 1 m for either scenario. The IMU movement model RMSE illustrates the advantage of using a step-based movement model where using just this movement model can outperform the state-of-the-art approach using the Rician movement model.

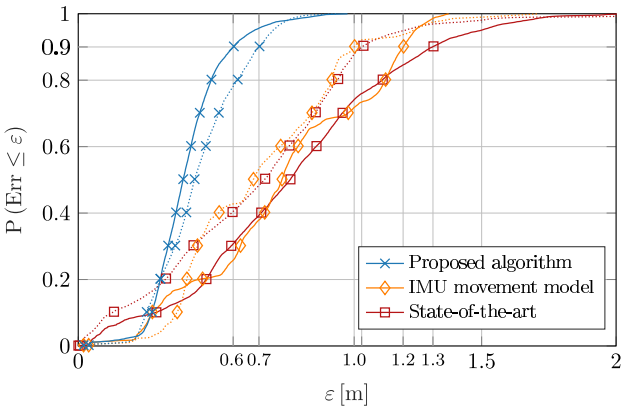


**FIGURE 7.** The empirical CDF of the RMSE $\varepsilon$ over the runs of the simulation. The proposed Channel-SLAM algorithm with data association provides significantly better performance than the state-of-the-art Channel-SLAM. The achieved precision of the IMU-based movement model without using the Channel-SLAM is shown by the orange line. The solid and dotted lines illustrate the first and the second scenarios, respectively. The additional grid lines mark the 90% confidence interval of the RMSE for each plot.

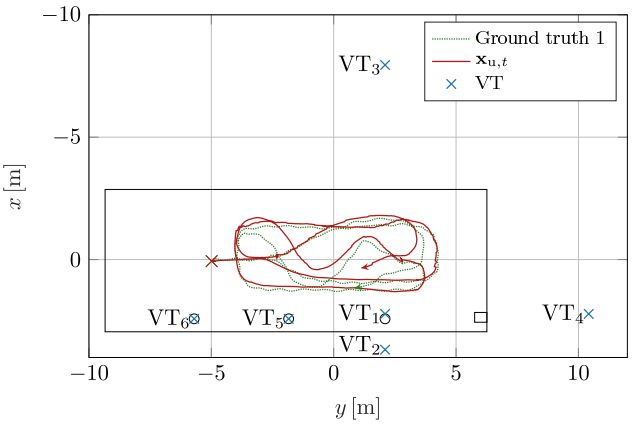


**FIGURE 8.** The layout of testing scenario number one with ground truth of the pedestrian movement and one realization of a proposed positioning algorithm with data association. The crosses mark the positions of four virtual transmitters. $VT_1$ is the position of the physical transmitter. Other VTs are caused by reflections from the room walls.

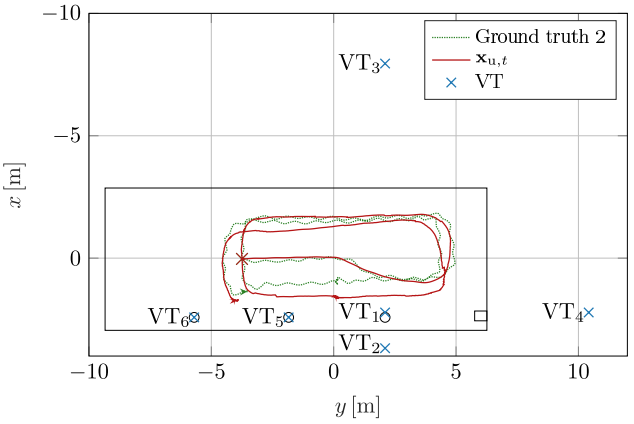


**FIGURE 9.** The layout of testing scenario number two with ground truth of the pedestrian movement and one realization of a proposed positioning algorithm with data association. The crosses mark the positions of four virtual transmitters. $VT_1$ is the position of the physical transmitter. Other VTs are caused by reflections from the room walls.

The empirical Cumulative Distribution Functions (CDFs) in Fig. 7 shows the overall comparison of the proposed Channel-SLAM algorithm with the state-of-the-art approach. The precision of the proposed algorithm outperforms the state-of-the-art approach in each simulated experiment. Also, we show the performance of the standalone IMU-based movement model to illustrate how the Channel-SLAM algorithm corrects movement model errors.

The additional grid lines mark the 90% confidence interval of the RMSE for each plot. For the first scenario, the 90% confidence interval of the proposed algorithm's RMSE is $\pm 0.58$ m, whilst for state-of-the-art it is $\pm 1.32$ m, and $\pm 1.21$ m is achieved using only the IMU-based movement model. For the second scenario, the 90% confidence interval of the proposed algorithm's RMSE is $\pm 0.67$ m, whilst for state-of-the-art it is $\pm 1.05$ m, and $\pm 1.03$ m is achieved using only the IMU-based movement model.

The computational complexity of the algorithms not only depend on the setting of the algorithm parameters, but also on the number of the MPCs, parameters of the MPCs, and the number of KEST outages. Based on a desktop computer using *MATLAB R2018b* implementation, we obtain the average duration of one run for the first scenario as 96.6 min for the proposed, and 91.3 min for the state-of-the-art algorithm, and for the second scenario 73.4 min and 71.5 min for the proposed and the state-of-the-art algorithm, respectively.

The comparison of the proposed Channel-SLAM algorithm with the state-of-the-art approach shows that the data association capability proposed in this work yields significantly better performance of the position estimation.

### C. EVALUATIONS OF PRECISION BASED ON MEASUREMENT

The MPCs extracted from the CIRs using the KEST algorithm are used as an input for the evaluation of the Channel-SLAM precision. Since we use the same recorded ground truth of the pedestrian movement together with the IMU data, we are able to compare the simulation with the performance achievable using low-cost hardware in a real scenario.

Fig. 8 and Fig. 9 show the recorded ground truth of the pedestrian movement and one realization of position estimation of measurement scenarios one and two, respectively. The values of the parameters used in the experiment are the same as the parameters used for the simulation, given in Table 10.

Fig. 10 shows the output of the KEST algorithm estimating the parameters of the MPCs from the recorded CIR during experiment scenario number one. The scatter plot color map indicates the estimated MPC magnitude. Additionally, based on the ground truth of the pedestrian movement, we show the calculated theoretical delay of the MPCs $MPC_1$–$MPC_6$ originating from $VT_1$–$VT_6$, respectively. The scatter plot shows more than the six MPCs. Those additional MPCs might be

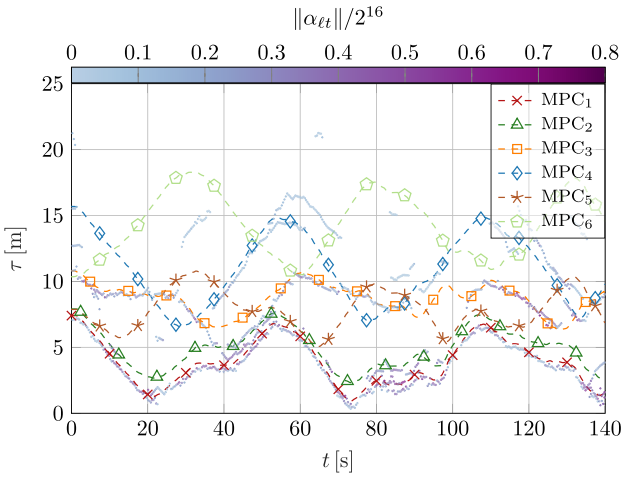


**FIGURE 10.** Comparison of the estimated CIR with the ground truth MPCs originating from VTs for scenario number one. The magnitude of the estimated CIR $\|\alpha_{\ell t}\|$ is shown by the scatter plot color. The receiver provides the amplitude measurement as a 16-bit number. The individual MPCs can be easily lost due to shadowing by the user's body and by other obstacles.

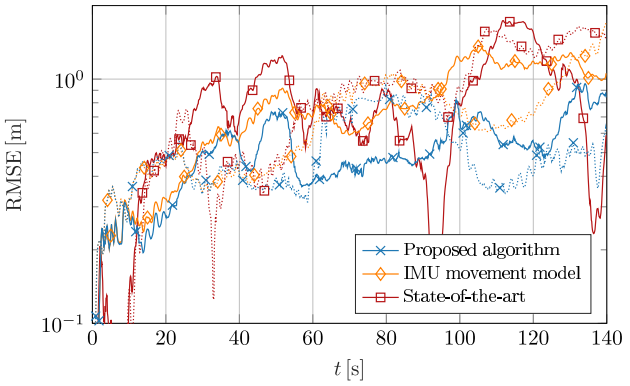


**FIGURE 11.** Comparison of the RMSE of the proposed Channel-SLAM algorithm and the state-of-the-art Channel-SLAM [20]. The achieved precision of the IMU-based movement model without using Channel-SLAM is shown by the orange line. The solid and dotted lines illustrate the first and the second scenarios, respectively.

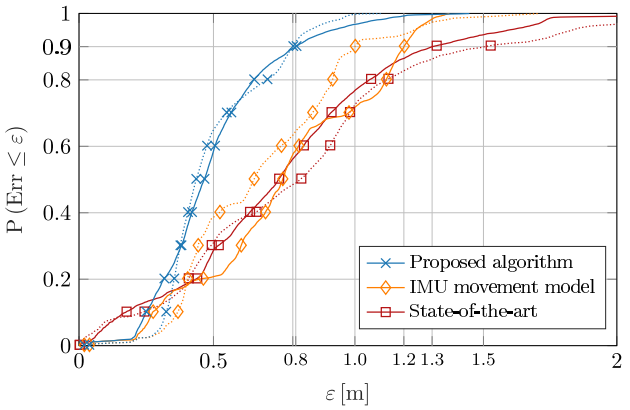


**FIGURE 12.** The empirical CDF of the RMSE $\varepsilon$ of the user position estimation. The proposed Channel-SLAM algorithm with data association provides significantly better performance than without the data association, or when using only the IMU-based movement model or the state-of-the-art Channel-SLAM. The values of maximal error for 90% probability interval are shown in the figure.

caused by multiple reflections of the transmitted signal, and by other scatterers. For the sake of plot readability, we show only $\text{MPC}_1$–$\text{MPC}_6$. However, the positioning algorithm is utilizing all of the available MPCs.

We can see that the calculated theoretical delay indicated by the dashed lines in Fig. 10 match the KEST estimate, when detectable. However, the MPCs are often distorted and cannot be tracked reliably all the time. Hence, the algorithm has to be robust to deal with outages that are occurring even more often when low-cost hardware is used compared to the professional broadband channel sounder used in [20].

Additionally, KEST may associate incorrect MPCs during the tracking. This is visible e.g., at $t = 35$ s, where $\text{MPC}_3$ is wrongly assigned and its delay continues to decrease. Since only $\text{MPC}_1$ and $\text{MPC}_3$ are observed, this faulty assignment would cause significant positioning error by steering the estimated position sideways.

However, this wrongly tracked MPC is successfully recognized by the KEST error detection algorithm described in Section III-A, and the KEST-based association is dropped. The effect of this algorithm is apparent in scenario one, marked using solid lines, in Fig. 11, where the RMSE of the state-of-the-art algorithm starts to increase, while the RMSE of the proposed data association algorithm starts to decrease shortly after.

The proposed Channel-SLAM algorithm improves the precision of the position estimation, as already mentioned in the previous paragraph. This is depicted in Fig. 11 where the comparison of the state-of-the-art approach with the proposed Channel-SLAM approach is illustrated using the RMSE. The solid and dotted lines illustrate the first and the second scenarios, respectively. The RMSE of the proposed algorithm never exceeds 1 m for both scenarios unlike the state-of-the-art approach exceeding 1 m in both scenarios. The IMU-based movement model RMSE illustrates how well the movement model inaccuracy is corrected using the CIR measurements.

The empirical CDFs in Fig. 12 show the overall comparison of the proposed Channel-SLAM algorithm with the state-of-the-art approach. The precision of the proposed algorithm outperforms the state-of-the-art approach in each experiment. Also, we show the performance of the standalone IMU-based movement model to illustrate how the Channel-SLAM algorithm corrects the movement model inaccuracy.

The additional grid lines mark the 90% confidence interval of the RMSE for each plot. For the first scenario, the 90% confidence interval of the proposed algorithm's RMSE is $\pm 0.81$ m, whilst for state-of-the-art it is $\pm 1.31$ m, and $\pm 1.21$ m is achieved using only the IMU-based movement model. For the second scenario, the 90% confidence interval of the proposed algorithm's RMSE is $\pm 0.80$ m, whilst for state-of-the-art is $\pm 1.50$ m, and $\pm 1.03$ m is achieved using only IMU-based movement model.

The average duration of one run for the first scenario is 54.5 min for the proposed, and 48.1 min for the state-of-the-art algorithm, and for the second scenario 59.2 min and 53.9 min for the proposed and the state-of-the-art algorithm, respectively.

The comparison of the proposed Channel-SLAM algorithm with the state-of-the-art approach shows that the data association capability proposed in this work yields significantly better precision of the position estimation.

When the low-cost UWB anchor is used, the MPCs are observed for a lower percentage of the time, and the outage can last longer compared to the professional broadband channel sounder used in [20]. During the KEST outage, the variance of user position increases, and when the MPCs re-occur, the initialization process creates new subordinate particle filters to start estimating the VT again. However, the variance of the user position is reflected in the variance of the VT via the initialization process. Thus, re-occurring VTs cannot improve the position estimation when the state-of-the-art approach is used for positioning. On the other hand, if the data association is performed, and some of the user position particles are associated with a previously observed VT, the variance of the position estimation decreases immediately. This process can recover the precision after an MPC outage.

The experiments were performed in a room with smooth walls and round scatterers. We do not expect the performance of the proposed algorithm to be negatively affected by an environment with rough walls and different shapes of scatterers. The experiment described in [19] was performed in an environment combining a lobby with glass walls and a meeting room with many edges around windows, which supports our belief.

## V. CONCLUSION

In this paper, we have proposed an improvement for the state-of-the-art Channel-SLAM algorithm and performed simulations and experiments using low-cost hardware to demonstrate the robustness of the proposed methods. It has been shown how the fusion of all available data provided by the IMU and signal measurement in a multipath radio channel allows positioning with only a single receiver and transmitter. On top of this, we can map the position of the physical transmitter, virtual transmitters, and scatterers. Finally, we compare our method with the state-of-the-art approach showing a substantial improvement of the precision.

The main improvements of the Channel-SLAM algorithm are a new movement model and a data association algorithm. The movement model, which incorporates the IMU measurements presented in Section III-B, increases the robustness of the algorithm when only a low number of MPCs are observed. The proposed data association method allows us to reuse the previously observed VTs and to provide a tool to deal with errors in the KEST labeling of MPCs. We also show a derivation of the Channel-SLAM algorithm jointly with data association. An interesting output of the derivation is the data association method, which is similar to the MHT obtained naturally during the derivation.

There are still open problems we need to address in future work. The low-cost UWB hardware has a low update rate causing changes of distance between measurements comparable with the wavelength of the carrier frequency, hence the linear model assumption used in KEST is violated for phase tracking. This nonlinearity causes the KF to be incapable of tracking the phase of the MPCs, which increases the probability of the KEST association error. Resolving this problem may be possible using a tight fusion of the UWB measurement with Channel-SLAM.

## REFERENCES

[1] W. H. Guier and G. C. Weiffenbach, "Genesis of satellite navigation," *Johns Hopkins*, vol. 18, no. 2, pp. 178–181, May 1997.

[2] *Enhancing Bluetooth Location Services With Direction Finding*, Bluetooth SIG, Kirkland, WA, USA, Jan. 2019.

[3] P. Bahl and V. N. Padmanabhan, "RADAR: An in-building RF-based user location and tracking system," in *Proc. IEEE INFOCOM Conf. Comput. Commun.*, vol. 2, Mar. 2000, pp. 775–784.

[4] M. Triki, D. M. Slock, V. Rigal, and P. Francois, "Mobile terminal positioning via power delay profile fingerprinting: Reproducible validation simulations," in *Proc. IEEE Veh. Technol. Conf.*, Melbourne, VIC, Australia, Sep. 2006, pp. 1–5.

[5] E. Kupershtein, M. Wax, and I. Cohen, "Single-site emitter localization via multipath fingerprinting," *IEEE Trans. Signal Process.*, vol. 61, no. 1, pp. 10–21, Jan. 2013, doi: 10.1109/tsp.2012.2222395.

[6] T. Deissler and J. Thielecke, "Feature based indoor mapping using a bat-type UWB radar," in *Proc. IEEE Int. Conf. Ultra-Wideband*, Vancouver, BC, Canada, Sep. 2009, pp. 475–479.

[7] T. Deissler and J. Thielecke, "UWB SLAM with rao-blackwellized Monte Carlo data association," in *Proc. Int. Conf. Indoor Positioning Indoor Navigat.*, Zurich, Switzerland, Sep. 2010, pp. 1–5.

[8] Y. Shen and M. Z. Win, "On the use of multipath geometry for wideband cooperative localization," in *Proc. GLOBECOM - IEEE Global Telecommun. Conf.*, Honolulu, HI, USA, Nov. 2009, pp. 1–6.

[9] M. Froehle, E. Leitinger, P. Meissner, and K. Witrisal, "Cooperative multipath-assisted indoor navigation and tracking (Co-MINT) using UWB signals," in *Proc. IEEE Int. Conf. Commun. Workshops (ICC)*, Atlanta, GA, USA, Jun. 2013, pp. 16–21.

[10] E. Leitinger, P. Meissner, M. Lafer, and K. Witrisal, "Simultaneous localization and mapping using multipath channel information," in *Proc. IEEE Int. Conf. Commun. Workshop (ICCW)*, London, U.K., Jun. 2015, pp. 754–760.

[11] E. Leitinger, F. Meyer, P. Meissner, K. Witrisal, and F. Hlawatsch, "Belief propagation based joint probabilistic data association for multipath-assisted indoor navigation and tracking," in *Proc. Int. Conf. Localization GNSS (ICL-GNSS)*, Barcelona, Spain, Jun. 2016, pp. 1–6.

[12] P. Meissner, E. Leitinger, and K. Witrisal, "UWB for robust indoor tracking: Weighting of multipath components for efficient estimation," *IEEE Wireless Commun. Lett.*, vol. 3, no. 5, pp. 501–504, Oct. 2014, doi: 10.1109/lwc.2014.2341636.

[13] K. Witrisal and P. Meissner, "Performance bounds for multipath-assisted indoor navigation and tracking (MINT)," in *Proc. IEEE Int. Conf. Commun. (ICC)*, Ottawa, ON, Canada, Jun. 2012, pp. 4321–4325.

[14] S. Thrun, W. Burgard, and D. Fox, *Probabilistic Robotics*, 1st ed. Cambridge, MA, USA: MIT Press, 2005.

[15] E. Leitinger, F. Meyer, F. Tufvesson, and K. Witrisal, "Factor graph based simultaneous localization and mapping using multipath channel information," in *Proc. IEEE Int. Conf. Commun. Workshops (ICC)*, Paris, France, May 2017, pp. 652–658.

[16] F. R. Kschischang, B. J. Frey, and H.-A. Loeliger, "Factor graphs and the sum-product algorithm," *IEEE Trans. Inf. Theory*, vol. 47, no. 2, pp. 498–519, Feb. 2001.

[17] C. Gentner and T. Jost, "Indoor positioning using time difference of arrival between multipath components," in *Proc. Int. Conf. Indoor Positioning Indoor Navigat.*, Montbeliard, France, Oct. 2013, pp. 1–10.

[18] C. Gentner, B. Ma, M. Ulmschneider, T. Jost, and A. Dammann, "Simultaneous localization and mapping in multipath environments," in *Proc. IEEE/ION Position, Location Navigat. Symp. (PLANS)*, Savannah, GA, USA, Apr. 2016, pp. 807–815.
[19] C. Gentner, T. Jost, W. Wang, S. Zhang, A. Dammann, and U.-C. Fiebig, "Multipath assisted positioning with simultaneous localization and mapping," *IEEE Trans. Wireless Commun.*, vol. 15, no. 9, pp. 6104–6117, Sep. 2016, doi: 10.1109/twc.2016.2578336.
[20] C. Gentner, R. Pöhlmann, M. Ulmschneider, T. Jost, and S. Zhang, "Positioning using terrestrial multipath signals and inertial sensors," *Mobile Inf. Syst.*, vol. 2017, pp. 1–18, 2017, doi: 10.1155/2017/9170746.
[21] Y. Bar-Shalom and X.-R. Li, *Multitarget-Multisensor Tracking: Principles and Techniques*, 1st ed. Storrs, CT, USA: Yaakov Bar-Shalom, 1995.
[22] S. Y. Cho and C. G. Park, "MEMS based pedestrian navigation system," *J. Navigat.*, vol. 59, no. 1, pp. 135–153, Dec. 2005, doi: 10.1017/s0373463305003486.
[23] J. H. Lee, B. Shin, C. Kim, J. Kim, S. Lee, and T. Lee, "Real time adaptive step length estimation for smartphone user," in *Proc. 13th Int. Conf. Control, Autom. Syst. (ICCAS )*, Gwangju, South Korea, Oct. 2013, pp. 382–385.
[24] M. Khedr and N. El-Sheimy, "A smartphone step counter using IMU and magnetometer for navigation and health monitoring applications," *Sensors*, vol. 17, no. 11, p. 2573, Nov. 2017, doi: 10.3390/s17112573.
[25] P. Bello, "Characterization of randomly time-variant linear channels," *IEEE Trans. Commun.*, vol. 11, no. 4, pp. 360–393, Dec. 1963, doi: 10.1109/TCOM.1963.1088793.
[26] G. L. Turin, F. D. Clapp, T. L. Johnston, S. B. Fine, and D. Lavry, "A statistical model of urban multipath propagation," *IEEE Trans. Veh. Technol.*, vol. 21, no. 1, pp. 1–9, Feb. 1972.
[27] T. Jost, W. Wang, U.-C. Fiebig, and F. Perez-Fontan, "Detection and tracking of mobile propagation channel paths," *IEEE Trans. Antennas Propag.*, vol. 60, no. 10, pp. 4875–4883, Oct. 2012, doi: 10.1109/TAP.2012.2207315.
[28] B. H. Fleury, M. Tschudin, R. Heddergott, D. Dahlhaus, and K. Ingeman Pedersen, "Channel parameter estimation in mobile radio environments using the SAGE algorithm," *IEEE J. Sel. Areas Commun.*, vol. 17, no. 3, pp. 434–450, Mar. 1999, doi: 10.1109/49.753729.
[29] T. S. Rappaport, *Wireless Communications—Principles and Practice*, 1st ed. Upper Saddle River, NJ, USA: Prentice-Hall, 1996.
[30] M. S. Arulampalam, S. Maskell, N. Gordon, and T. Clapp, "A tutorial on particle filters for online nonlinear/non-Gaussian Bayesian tracking," *IEEE Trans. Signal Process.*, vol. 50, no. 2, pp. 174–188, Aug. 2002, doi: 10.1109/78.978374.
[31] P. Kozierski, M. Lis, and J. Zietkiewicz, "Resampling in particle filtering—Comparison," *Studia Automatyki Informatyki*, vol. 38, pp. 35–64, Jan. 2013.
[32] M. Ulmschneider, C. Gentner, T. Jost, and A. Dammann, "Multiple hypothesis data association for multipath-assisted positioning," in *Proc. 14th Workshop Positioning, Navigat. Commun. (WPNC)*, Bremen, Germany, Oct. 2017, pp. 1–6.
[33] S. Thrun, M. Montemerlo, D. Koller, B. Wegbreit, J. Nieto, and E. Nebot, "Fastslam: An efficient solution to the simultaneous localization and mapping problem with unknown data association," *J. Mach. Learn. Res.*, vol. 2004, pp. 380–407, May 2004.
[34] B. Krach and P. Robertson, "Integration of foot-mounted inertial sensors into a Bayesian location estimation framework," in *Proc. 5th Workshop Positioning, Navigat. Commun.*, Hannover, Germany, Mar. 2008, pp. 55–61.
[35] A. Martinelli, H. Gao, P. D. Groves, and S. Morosi, "Probabilistic context-aware step length estimation for pedestrian dead reckoning," *IEEE Sensors J.*, vol. 18, no. 4, pp. 1600–1611, Feb. 2018, doi: 10.1109/jsen.2017.2776100.
[36] Y. Bar-Shalom, X.-R. Li, and T. Kirubarajan, *Estimation With Applications to Tracking and Navigation: Algorithms and Software for Information Extraction*, 1st ed. New York, NY, USA: Wiley, 2001.
[37] O. J. Woodman, "An introduction to inertial navigation," Comput. Lab., Cambridge, U.K., Tech. Rep. 696, 2007.
[38] D. Hilbert and S. Cohn-Vossen, *Geometry and the Imagination*, 2nd ed. Providence, RI, USA: AMS Chelsea, 1999.
[39] R. Kulhavý and M. B. Zarrop, "On a general concept of forgetting," *Int. J. Control*, vol. 58, no. 4, pp. 905–924, Oct. 1993, doi: 10.1080/00207179308923034.
[40] P. M. Djuric, J. Kotecha, J. Tourneret, and S. Lesage, "Adaptive signal processing by particle filters and discounting of old measurements," in *Proc. ICASSP*, Salt Lake City, UT, USA, 2001, pp. 3733–3736 vol. 6.
[41] V. Smidl and F. Gustafsson, "Bayesian estimation of forgetting factor in adaptive filtering and change detection," in *Proc. IEEE Stat. Signal Process. Workshop (SSP)*, Ann Arbor, MI, USA, Aug. 2012, pp. 197–200.
[42] M. Kárný, "Approximate Bayesian recursive estimation," *Inf. Sci.*, vol. 285, pp. 100–111, Nov. 2014, doi: 10.1016/j.ins.2014.01.048.
[43] C. Gentner and M. Ulmschneider, "Simultaneous localization and mapping for pedestrians using low-cost ultra-wideband system and gyroscope," in *Proc. Int. Conf. Indoor Positioning Indoor Navigat. (IPIN)*, Saporo, Japan, Sep. 2017, pp. 1–8.

**ROSTISLAV KARÁSEK** received the B.Sc. and M.Sc. degrees focusing on the topic of wireless communications from the Czech Technical University in Prague, in 2015 and 2017, respectively.

During his study, he received practical experience at the Valeo Prague Research and Development Center. Since 2019, he has been completing his Ph.D. degree with the Institute of Communications and Navigation, German Aerospace Center (DLR), where he obtained a DAAD Scholarship. His research interests include the propagation of the electromagnetic field and its utilization for indoor positioning.

**CHRISTIAN GENTNER** received the Dipl. Ing. (BA) degree in electrical engineering, focusing on the main topic of communication technology, from the University of Applied Science Ravensburg-Weingarten, in 2006, and the M.Sc. and Dr. Ing. (Ph.D.) degrees in electrical engineering from the University of Ulm, in 2009 and 2018, respectively.

During his BA study, he received practical experience at Rohde & Schwarz in Munich. Since 2009, he has been working at the Institute of Communications and Navigation, German Aerospace Center (DLR). His current research focuses on indoor positioning.